NsG-58-60

113p.

N64-25566

CODE-1 CAT. 28

NASA CR-56828

OTS PRICE

XEROX $ 9.60 ph

MICROFILM $ _____

UNIVERSITY OF MARYLAND
DEPARTMENT OF PHYSICS AND ASTRONOMY
COLLEGE PARK, MARYLAND

UNPUBLISHED PRELIMINARY DATA

RC# 19

THE TIME DEPENDENCE OF RADIATION BELT LIFETIMES AND SOME APPLICATIONS

by

Forrest E. England

Thesis submitted to the Faculty of the Graduate School of the University of Maryland in partial fulfillment of the requirements for the degree of
Master of Science
1964

APPROVAL SHEET

Title of Thesis: The Time Dependence of Radiation Belt Lifetimes and Some Applications

Name of Candidate: Forrest Edwin England
Master of Science, 1964

Thesis and Abstract Approved: _____
S. F. Singer
Professor
Physics

Date Approved:

ABSTRACT

25564

Title of Thesis: The Time Dependence of Radiation Belt Lifetimes and Some Applications

Forrest Edwin England, Master of Science, 1964

Thesis Directed by: S. F. Singer, Professor of Physics

The lifetimes of particles in the radiation belt vary as a consequence of fluctuations of the loss processes such as produced by variations of atmospheric density with time. The time scale of atmospheric variations affects the averaged atmospheric density to which trapped particles are exposed and therefore determines the time dependence of the radiation lifetimes as set by the atmosphere.

Since observations are usually made of the radiation flux rather than of lifetime, a number of models of injection and loss, which determine the resultant flux, are examined. Special cases of injection and removal are considered. Artificial injections such as Starfish can be used to investigate the particle lifetimes. Similarly, artificial removal by sweeper satellites is shown to modify the radiation belt in such a way as to enable physical properties of the radiation belt and its environment to be deduced.

Author

VITA

Name: Forrest Edwin England

Permanent Address: 714 Cottonwood Drive, Severna Park, Maryland

Degree and date to be conferred: Master of Science, 1964

Date of birth: [redacted]

Place of birth: [redacted]

Secondary Education: Stuyvesant High School, New York City;
Roslyn High School, Roslyn, Long Island

Collegiate institute attended	Date	Degree	Date of Degree
The Cooper Union	1951-55	B.M.E.	1955

Positions held: Junior Engineer, Associate Engineer, Engineer and Senior Engineer
Mechanical Design and Development
Westinghouse Electric Corporation
Aerospace Division
Baltimore, Maryland
1955 to present

ACKNOWLEDGMENTS

The author wishes to express his appreciation to Dr. Singer for suggesting the thesis topic and for helpful counsel during its preparation.

Thanks are also expressed to Mr. Alexander Nagy, whose encouragement and considerations are deeply appreciated.

I wish to thank the many persons who assisted in the typing and other matters so that this thesis could be completed.

Finally, appreciation of my wife's patience and endurance, an invaluable ingredient of this thesis, is acknowledged.

This work was supported in part by NASA Grant 58-60.

Page intentionally left blank

TABLE OF CONTENTS

Section		Page
APPENDIX A.	B-L COORDINATES	79
APPENDIX B.	AVERAGE DENSITY	87
REFERENCES		94

LIST OF FIGURES

Figure		Page
1	Störmer's Allowed and Forbidden Regions.	4
2	The Radiation Belt	6
3a	Characteristic Times for Trapped Particles in the Geomagnetic Field	12
3b	Characteristic Times for Trapped Particles in the Geomagnetic Field	13
3c	Characteristic Times for Trapped Particles in the Geomagnetic Field	14
3d	Characteristic Times for Trapped Particles in the Geomagnetic Field	15
3e	Characteristic Times for Trapped Particles in the Geomagnetic Field	16
4	Proton Lifetimes	24
5	Particle Concentration With Steady Injection and Constant	28
6	Particle Concentration With Impulsive Injection and Constant τ, Small n_o	28
7	Particle Concentration With Impulsive Injection and Constant τ, Large n_o	30
8	Particle Concentration With a Step Removal and Constant Injection.	30
9	Particle Concentration With Impulsive Removal and Constant Injection.	32
10	Particle Concentration With Steadily Increasing Removal and Constant Injection.	32

LIST OF FIGURES

Figure		Page
11	Particle Concentration With a Small Oscillating Removal and Constant Injection	35
12	Particle Concentration With a Large Oscillating Removal and Constant Injection	35
13	Proton Lifetimes as Limited by Energy Loss in the Atmosphere and by the Effect of a Sweeper Satellite	40
14	Satellite Orbit and Particle Orbit in an Eccentric Magnetic Field	42
15	Particle Concentrations in the Vicinity of a Swept Region	50
16	Particle Orbit Intersecting Swept Region	53
17	Absorption Fraction vs Separation From Swept Region	53
18	Detail of Flux Profile	58
19	Sweeper Limited Flux: Atmospheric Limited Flux vs Energy	58
20	Calculated Decay of Starfish Electrons (L = 1.25, E = 2.25 Mev) (from Welch, et al. (1963))	65
21	Comparison of Natural Decay and Hypothetical Sweeper Decay of Starfish Electrons	67
22	Averaged Atmospheric Density $\bar{\rho}$ vs $\omega\tau$	71
23	Proton Flux Variations	76
24	Magnetic Shells in a Dipole Field	80
25	Magnetic Coordinates for a Dipole Field	85

LIST OF FIGURES

Figure		Page
26	Mirror Point Trace in Real Field	89
27	Average Atmospheric Density* vs Geocentric Distance .	90

LIST OF TABLES

Table		Page
I	Characteristic Times for Trapped Particles in the Geomagnetic Field	17
II	Atmospheric Density Conversion	21
III	Proton Lifetimes in a Swept Environment $A_S \tau_S$ (cm^2 - sec.)	48
IV	Energy Dependence of $j_s/j_{atm} \sim E^n$	59
V	Observed Proton Flux Variations With Time	73
VI	McIlwain's Coordinate Transformation	82
VII	Average Atmospheric Density (Effective Electrons Per cm^3) on Lines of Force (L = 1.297, B_m = .186 gauss)	91
VIII	Real Field Average Density vs Dipole Model Density (L = 1.297, B_m = .186 gauss)	93

LIST OF SYMBOLS

a	Gyroradius of trapped particle
A	Area of current loop
A_S	Sweeper area
B	Magnetic field strength, gauss
B_m	Magnetic field strength at mirror point
c	Velocity of light
d	Diameter of sweeper
e	Electronic charge
E	Kinetic energy of trapped particle, Mev
f	Force
H_o	Atmospheric scale height
I	Longitudinal invariant
I'	Reduced Longitudinal invariant
j	Particle flux, $cm^2\ sec^{-1}\ ster^{-1}$
j_o	Injection rate of particles
K	Loss factor
L	Magnetic shell parameter
m	Rest mass of particle
M	Proton rest mass
n	Concentration of charged particles

LIST OF SYMBOLS

p	Momentum of particle
P	Probability that a given particle collides with a sweeper satellite
q	Electrical charge
r_e	Equatorial radius of line of force
r_o	Classical electron radius
R	Earth's radius
R_s	Orbital radius of sweeper satellite
S	Spiral path length
t	Time
T_{ns}	Time for North-South oscillation
v	Particle velocity
v_d	Drift velocity of particle
V	Volume
Z	Atomic number of absorber
Z	Length along line of force
α	Pitch angle of charged particle
β	v/c
γ	$(1 - \beta^2)^{-1/2}$
Δ	Eccentricity of dipole center in geographic coordinates
ϵ	Fractional variation of atmospheric density
θ	Deflection of charged particle

LIST OF SYMBOLS

θ	Coordinate describing intersection of sweeper orbit and equatorial crossing region allowed for particle
Θ	Phase of cycle for atmospheric variations
λ	Latitude in magnetic coordinates
λ_d	Debye shielding distance
Λ	Slowly varying log term related to absorber material material
μ	Magnetic moment of trapped particle
ρ	Atmospheric density
$\bar{\rho}$	Averaged atmospheric density
ρ_o	Mean atmospheric density
σ_N	Nuclear cross section
τ	Lifetime of particle
Φ	Flux invariant
ω	Frequency of atmospheric variation
ω_d	Angular drift of trapped particle

SECTION I

INTRODUCTION AND BACKGROUND

A. Introduction

It has been only a few years since the discovery of the natural radiation belts by artificial satellite culminated the ground work of men like Birkeland, Störmer, Alfvén, and others. In the brief period since that time a considerable effort has been made to understand more fully the nature of the belts, and the source of their origin. In particular, numerous instrumented artificial satellites have been launched to measure the flux and energy of the trapped particles. Other particles have been injected artifically by high altitude nuclear explosions and their behavior in the trapped region has been predicted and observed.

It is the purpose of this work to contribute to this growing fund of knowledge by examing the time dependence of the radiation lifetime including several related topics and to indicate their significance.

Since a flux measurement reflects the net effect of injection and of lifetime of the particles, it is essential that suitable models of lifetimes be combined with probable models of injection so that a meaningful interpretation of observed data may be obtained.

In the remainder of this section, a brief chronology of the work in this area leading up to the present time is given. As a further

introduction to the main issue, the fundamentals of the particle motions and the loss mechanisms are reviewed in Section II.

The various models of injection and removal, with their resultant effect on the measured flux levels are treated in Section III.

Section IV considers a number of special cases including artificial injection and removal, and the effect of atmospheric variations on the lifetimes. A related topic, interpretation of a modified radiation belt as caused by the sweeping action of a satellite, is treated in this section also.

B. The Radiation Belt

The radiation belt consists of energetic protons and electrons which are trapped by the earth's magnetic field. The extent of the belt is several earth radii within about 25° of the magnetic equator, and has the general shape of a donut with a crescent-shaped cross-section. The protons have energies up to several hundred Mev, the electrons up to several Mev (O'Brien, et al, 1962).

The existence of the radiation belt has been confirmed only recently, with the advent of artificial satellites (Van Allen, et al, 1958 a). Experimental and theoretical work had preceded the discovery by about sixty years. The very first experiments were conducted by Birkeland at the turn of the century in order to explain the polar aurora. He observed electrical discharges near a small magnetized sphere, representing the earth. Poincaré (1896) used a monopole and observed that

a charged particle would approach to a minimum distance and be repulsed. Störmer continued by examining the behavior of a charged particle which approached a dipole field instead of a monopole, the former being more truly representative of the earth's field. One of the significant conclusions which Störmer made was that a charged particle approaching from infinity could not stay in the earth's vicinity, (i.e. be trapped); it must return to infinity or collide with the earth. In the process of his analysis, he developed a map of allowed and forbidden regions for a given particle which was related to the dipole moment and the particle's energy. Under some conditions, an allowed region adjacent to the earth existed which was separated from infinity by a strip of the forbidden region as shown in Figure 1. This inner allowed region resembled a donut with a crescent shaped cross section. Störmer assumed that this region was inaccessible, hence it was empty.

Later, Alfvén extended Störmer's work and applied it to the solar-interplanetary magnetic field suggesting that cosmic rays might be scattered into inner solar allowed regions, and thereby become trapped in the solar dipole field. Singer (1957) suggested a similar situation for the earth's field and worked out the dynamics of trapped particle motion. He assumed that charged particles of solar origin could perturb the earth's field sufficiently to allow a portion of the particles in a stream to become trapped at a distance of several earth radii; Singer (1956) also considered briefly injection of cosmic ray

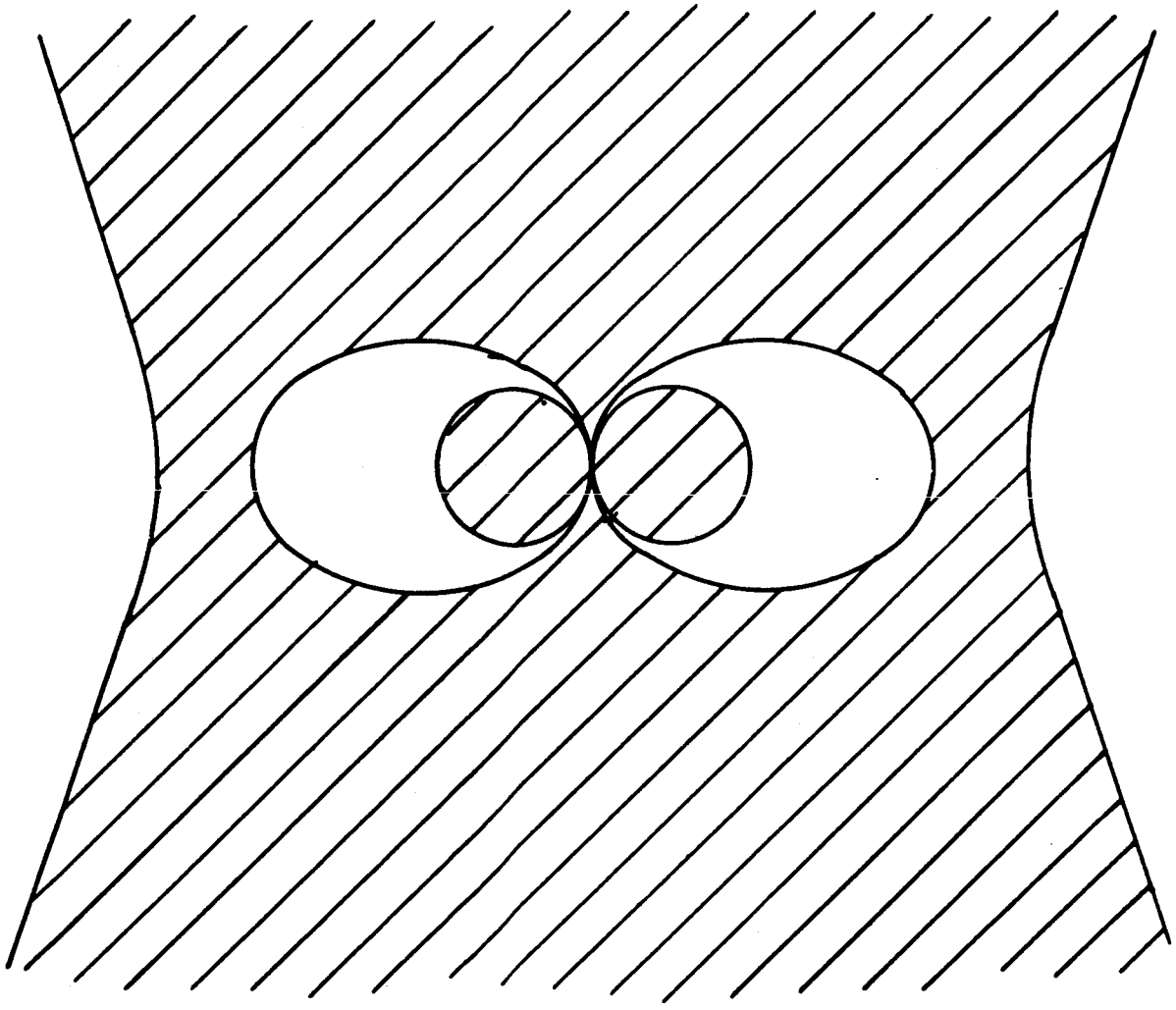

Figure 1. Störmer's Allowed and Forbidden Regions

albedo. Soon after the discovery of radiation at about 1000 KM above sea level, it was suggested that the trapped radiation was not electrons of solar origin but high energy protons produced from cosmic ray neutron albedo (Singer 1958 a, b; Vernov et al, 1959; Kellogg, 1959). Singer predicted a belt of high energy protons with energies up to several hundred Mev in the region between one and two earth radii. The existence of these "hard" protons was confirmed by a recovered nuclear emulsion exposed in a Thor-Able nose cone (Freden and White, 1959) and the extent of the region was confirmed by other experiments (Van Allen and Frank 1959 a; and Fan, Meyer and Simpson 1961). Refer to Figure 2.

The principles of the trapping of charged particles have become familiar and well understood. The origin of the trapped radiation is less well understood, however. The only source mechanism that has been successfully investigated in quantitative terms is the neutron albedo theory (Singer and Lenchek, 1962; Lenchek, 1962).

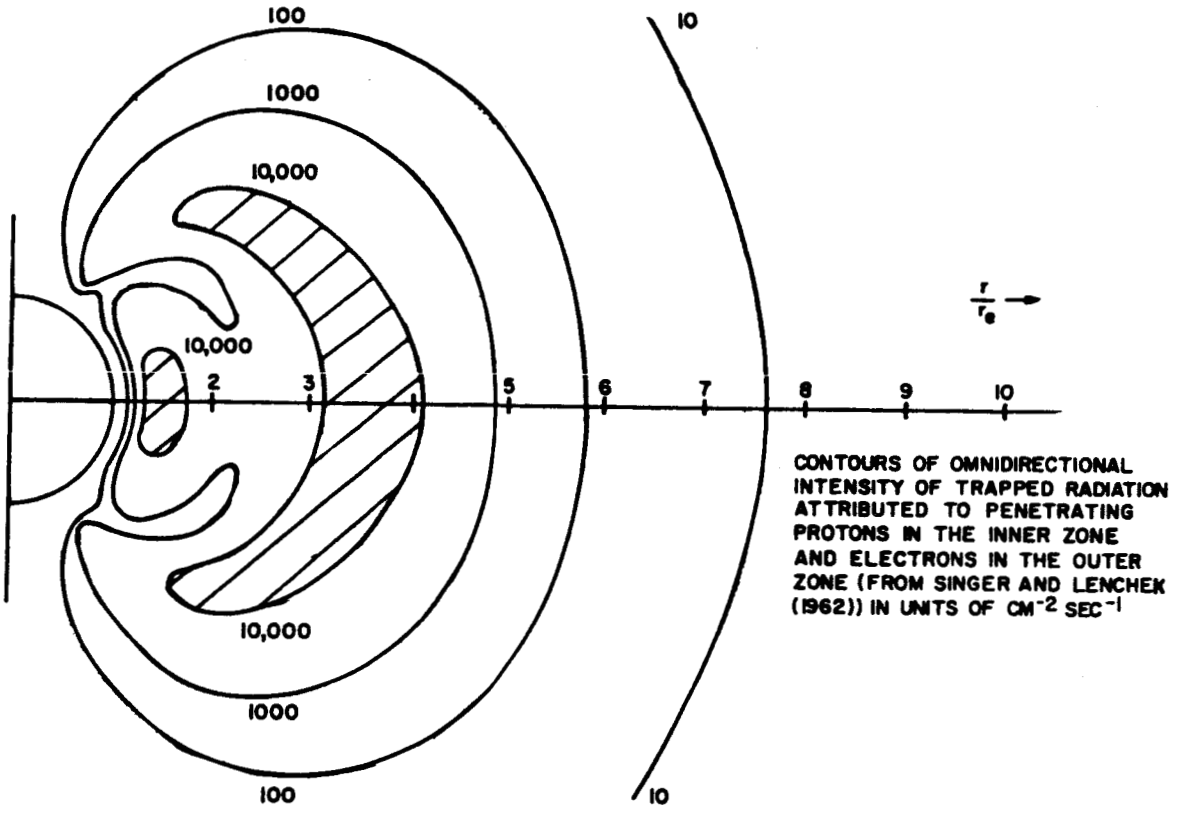

Figure 2. The Radiation Belt

SECTION II

FUNDAMENTALS OF TRAPPED RADIATION

A. Motion of Charged Particles in the Radiation Belts

For many considerations of particle motion in the earth's magnetic field it has been found suitable to approximate the field by a dipole model. This simplification has enabled the general features of the motion to be more easily described, and in many cases it has not detracted from physical reality. A starting point for this discussion is the familiar basic motion of a charged particle in a magnetic field.

A particle with velocity $\vec{v}$ and charge q moving in such a magnetic field experiences a force

$$\vec{F} = q \vec{v} \times \vec{B} \qquad (1)$$

where: B = total magnetic field strength.

This force, acting orthogonally to the field and velocity vectors, causes the particle to describe a circular path of radius

$$a = \frac{m \gamma v_{\perp}}{q B} = \frac{m \gamma v}{q B} \sin \alpha \qquad (2)$$

where

$$\gamma = (1 - \beta^2)^{-1/2}$$

$$\beta = v/c$$

$$v_{\perp} = v \sin \alpha$$

α = pitch angle, between $\vec{B}$ and $\vec{v}$

m = rest mass of particle

For values of α other than 90°, the particle has a component of velocity parallel to the field line. Therefore, the total motion consists of a rapid circling motion and a drift of the "guiding center" along the field line. It is assumed the magnetic field does not change appreciably over the dimension of the circle or within a gyroperiod.

The circular motion produces a current loop with a magnetic moment μ:

$$\mu = IA$$

$$= (1/2\ m\ v^{2}/B)\gamma \qquad (3)$$

For changes of B which are sufficiently small in space and time, the motion will be periodic, and μ is an adiabatic invariant (Alfvén, 1950; Spitzer, 1956). It is therefore required that

$$\frac{dB}{dt} \ll \frac{B}{t_g} = \frac{q\ B^2}{2\pi m\gamma} \qquad (4)$$

and

$$\frac{|\nabla B|}{B} \ll \frac{1}{a}$$

where the gyroperiod is

$$t_g = \frac{2\pi\ m\gamma}{q\ B}$$

For μ constant, an important feature of the motion is the reflection of a particle from a region with increased field strength:

$$\mu = \text{constant} = (1/2\ mv^2 \sin^2 \alpha/B)\gamma = E_\perp/B \qquad (5)$$

In the absence of magnetic fluctuations, the particle's energy remains constant and can be removed from the expression without altering its significance.

$$\therefore \frac{\sin^2 \alpha}{B} = \text{constant} = \frac{1}{B_m} \qquad (6)$$

The field strength B_m is the value at the point where the pitch angle passes through 90° and the particle is reflected.

The path length traveled by the particle as its guiding center moves along the field line from the equator to its mirror point has been approximated by Wentworth [1960] :

$$S(\alpha_e) \approx 1.38 - 0.32 \left[\sin \alpha_e + \sin^{1/2} \alpha_e\right] \qquad (7)$$

The path length is expressed in terms of the equatorial radius to the guiding center, and α_e is the equatorial pitch angle. The bounce period is determined from the particle's velocity, which remains unchanged in a static field, and the path length:

$$t_b = \frac{4S(\alpha_e)\, r_e}{\beta c} \qquad (8)$$

The bounce period is seen to be energy dependent and only slightly dependent on the pitch angle.

Another important feature of the motion is drift due to forces on the particle which are at right angles to the field vector. A particle

acted on by a small force $\vec{f}$ will drift at right angles to $\vec{f}$ and $\vec{B}$ with velocity v_D (Alfvén 1950):

$$\vec{v}_D = \frac{\vec{f} \times \vec{B}}{q B^2} \tag{9}$$

Drift forces may be magnetic, electrical, gravitational or inertial in origin. One that is significant to this discussion is the inertial force on a particle tending to follow a line of force in the earth's field. Because of the curvature of the line, a centrifugal force appears to act on the particle causing it to drift either to the east or the west, depending on the polarity of its charge.

$$\vec{v}_{D1} = m \gamma v^2 \cos^2 \alpha \frac{\vec{R}_c \times \vec{B}}{q B^2 R_c^2} \tag{10}$$

where: R_c = radius of curvature of field line.

For a nonhomogeneous magnetic field, the variation of the gyroradius around the path also causes drift:

$$\vec{v}_{D2} = 1/2\, m \gamma v^2 (\sin^2 \alpha) \frac{\vec{B} \times (\nabla_\perp B)}{q B^3} \tag{11}$$

where: $\nabla_\perp B$ is the component of $\nabla \vec{B}$ which is perpendicular to $\vec{B}$.

Equation 10 can be rewritten (Singer & Lenchek [1962]) if a static field with negligible current is assumed, i.e. $\nabla \times B = 0$.

$$\vec{v}_{D1} = m \gamma v^2 (\cos^2 \alpha) \frac{\vec{B} \times (\nabla_\perp \vec{B})}{q B^3} \tag{12}$$

Summing v_{D1} and v_{D2} and expressing energy in terms of the rest energy $E' = E/mc^2$,

$$v_D = 1/2\ mc^2 \frac{E'(E'+2)}{E'+1} \frac{\vec{B} \times (\nabla_\perp \vec{B})}{q B^3} (1 + \cos^2 \alpha) \qquad (13)$$

For $\beta << 1$ and for particles confined near the equator,

$$v_D = 1.51 \times 10^3\ E\ (r_e/R)^2\ \text{cm sec}^{-1}$$

where

E = keV

r_e = equatorial radius of field line

R = earth's radius

The average angular drift rate is given by (Hamlin et al. (1961))

$$\omega_D \approx \frac{3m}{q B_e r_e^2} \frac{v^2}{(1 - v^2/c^2)^{1/2}} \left[0.35 + 0.15 \sin \alpha_e\right]$$

$$= \frac{mc^2 \gamma \beta^2}{q B_e r_e^2} \left[1.05 + 0.45 \sin \alpha_e\right] \qquad (14)$$

Drift is westward for positively charged particles in the earth's field. The drift period is noted to be energy dependent and slightly pitch angle dependent.

These characteristic times are summarized in Table I and presented in graphical form in Figure 3.

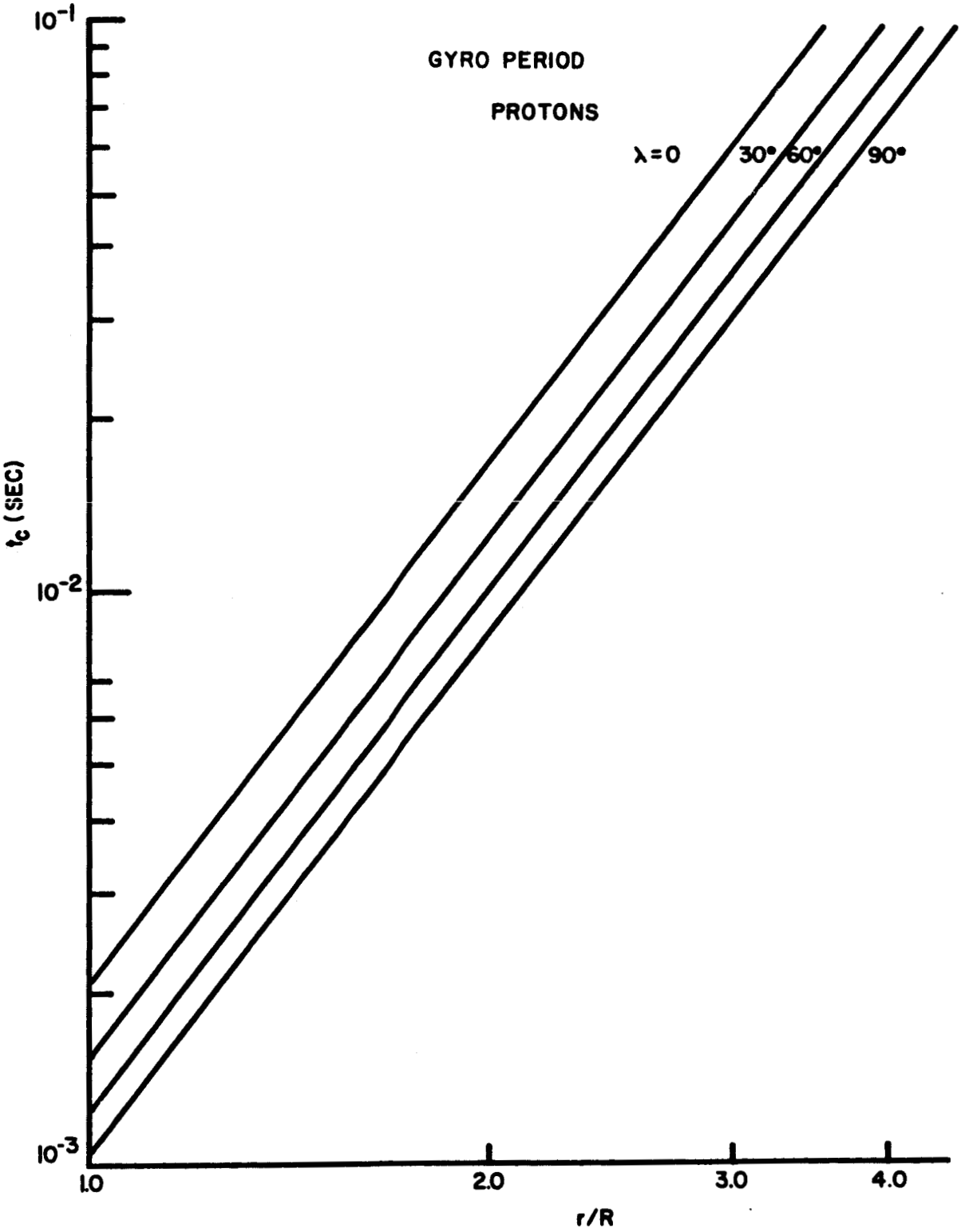

Figure 3a. Characteristic Times for Trapped Particles in the Geomagnetic Field

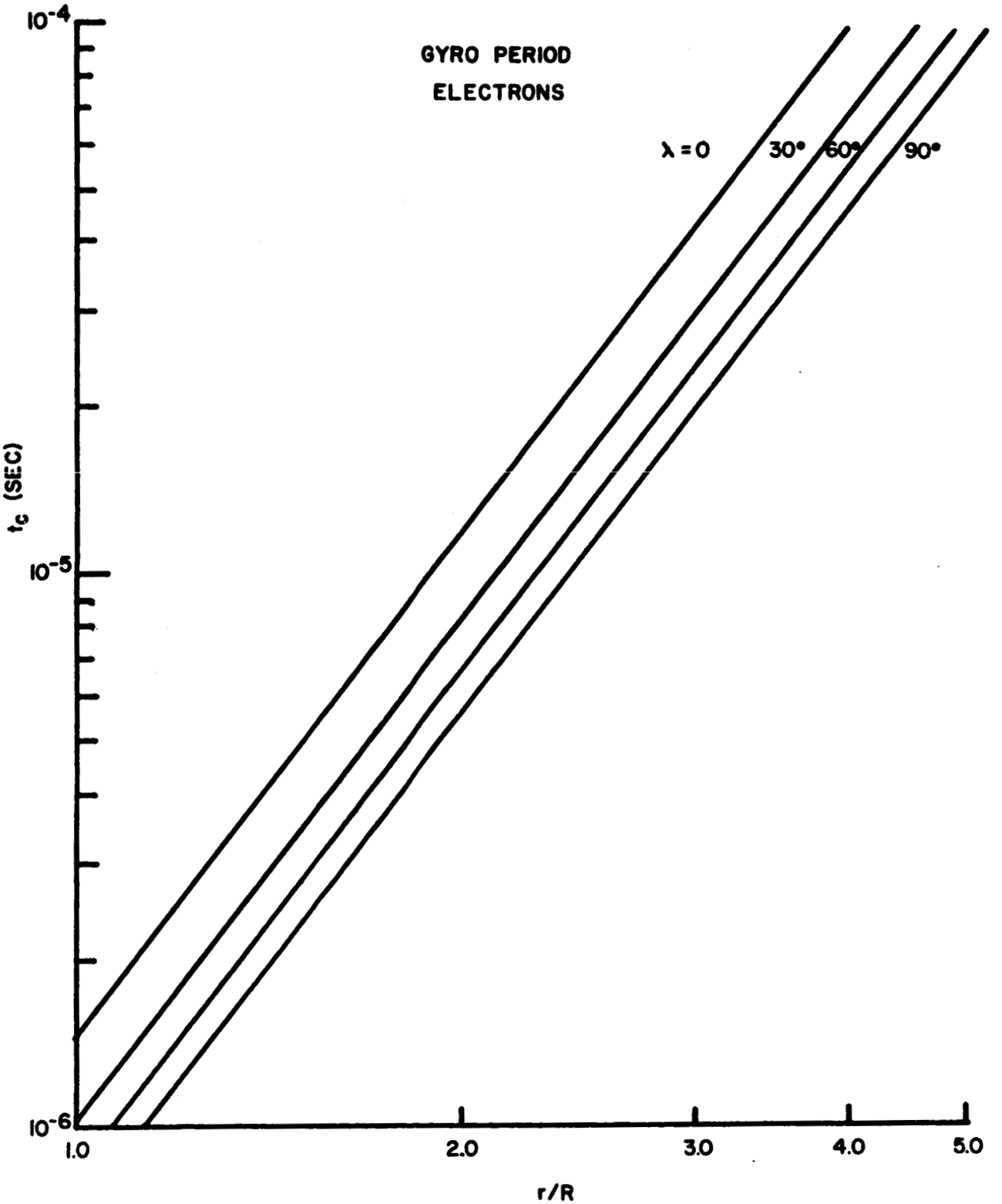

Figure 3b. Characteristic Times for Trapped Particles in the Geomagnetic Field

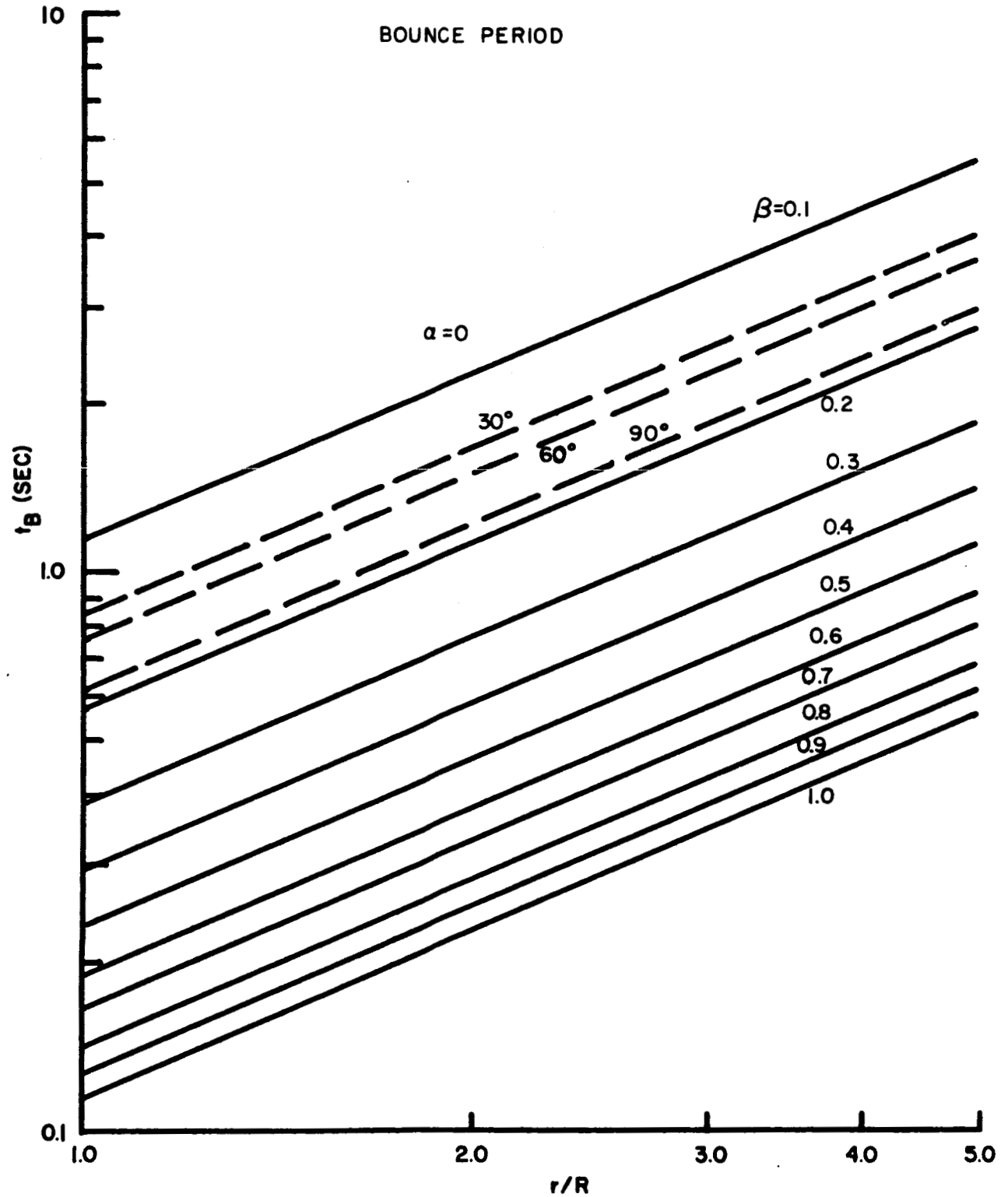

Figure 3c. Characteristic Times for Trapped Particles in the Geomagnetic Field

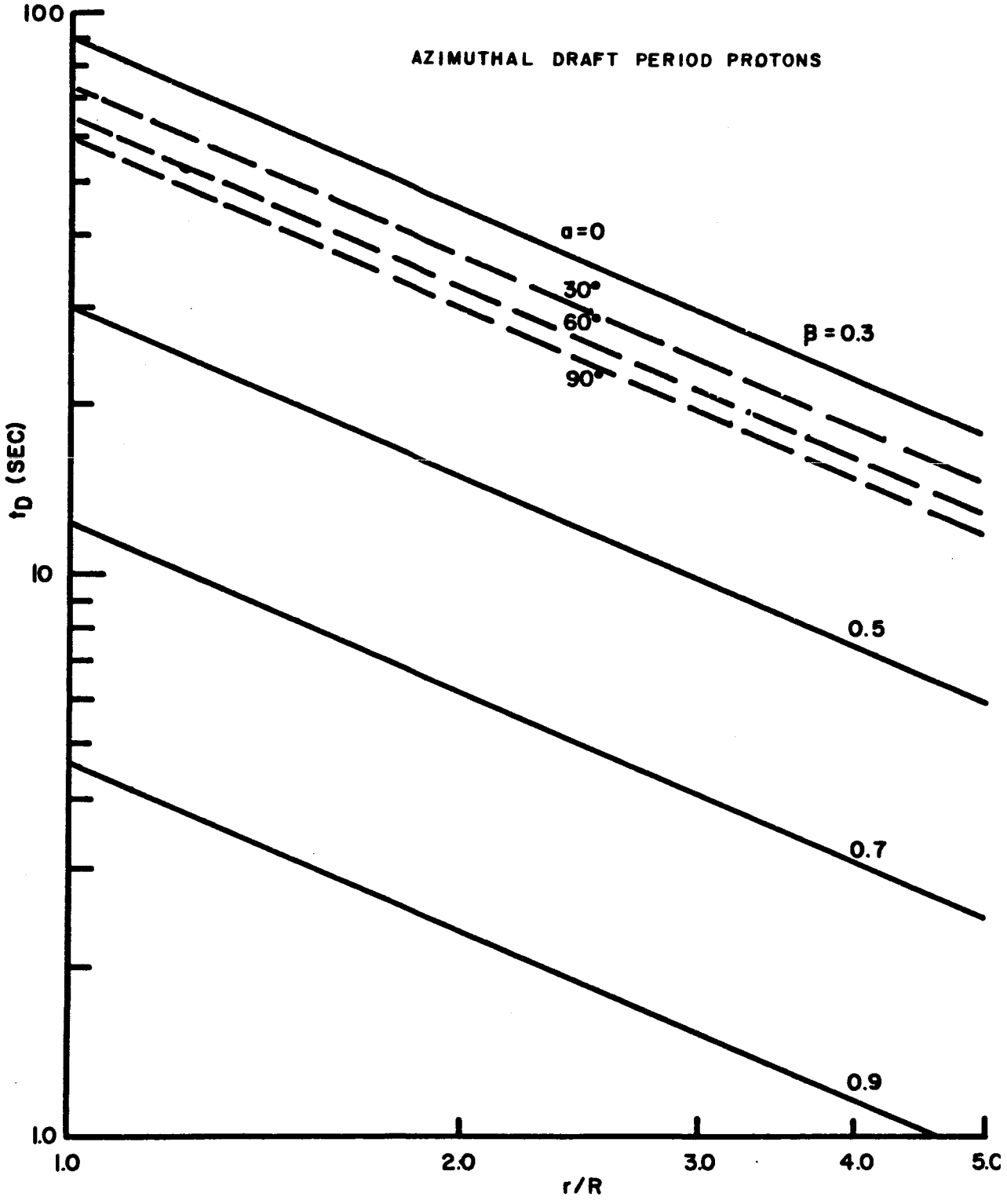

Figure 3d. Characteristic Times for Trapped Particles in the Geomagnetic Field

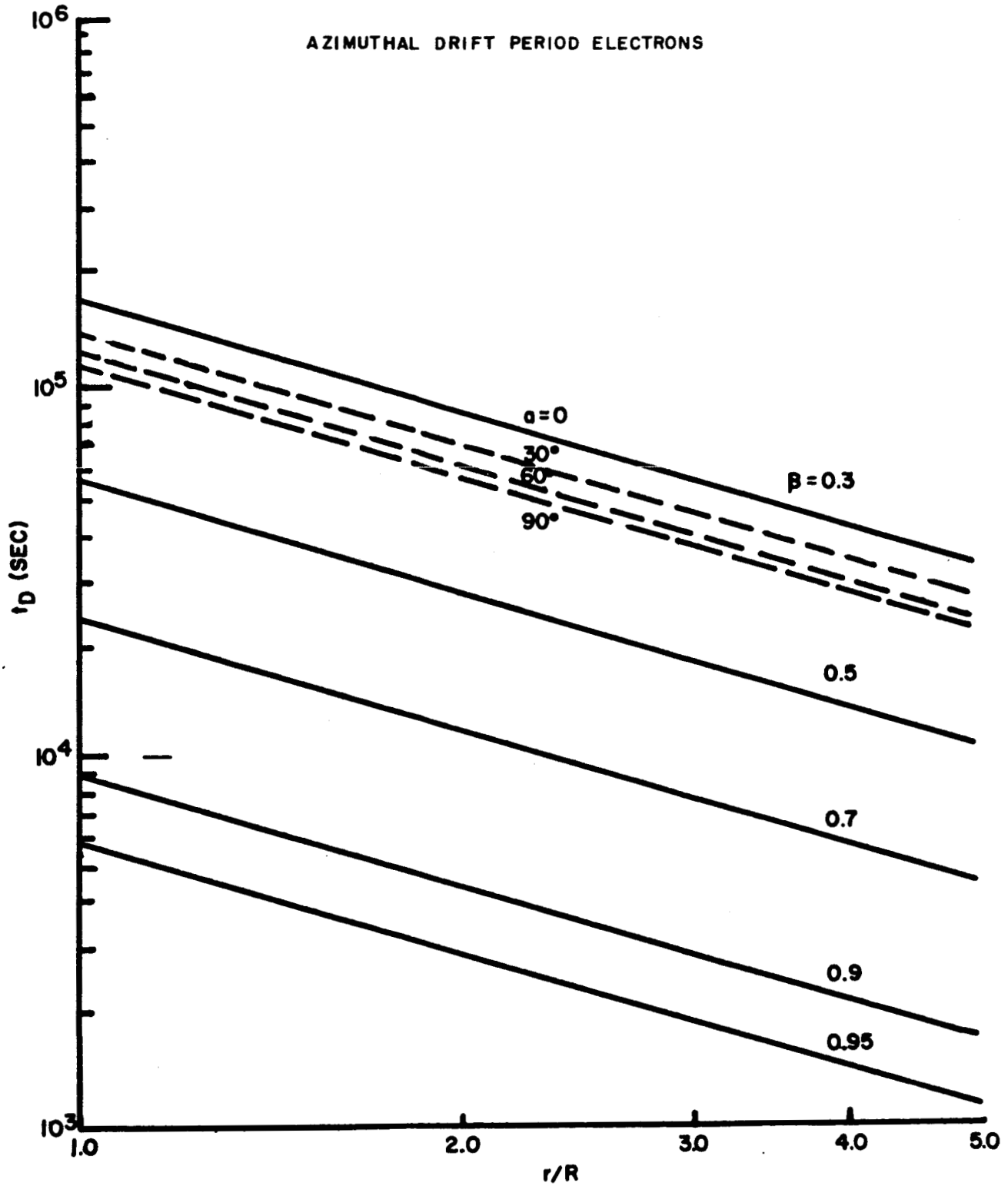

Figure 3e. Characteristic Times for Trapped Particles in the Geomagnetic Field

TABLE I

CHARACTERISTIC TIMES FOR TRAPPED PARTICLES IN THE GEOMAGNETIC FIELD*

Gyro period, t_c (sec, B in gauss)

protons: $6.5 \times 10^{-4}/B = 2.1 \times 10^{-3} (r/R)^3 /(4-3 \cos^2 \lambda)^{1/2}$

electrons: $3.55 \times 10^{-7}/B = 1.14 \times 10^{-6} (r/R)^3 /(4-3 \cos^2 \lambda)^{1/2}$

Bounce period, t_b

$$0.117 (L/\beta) \left[1 - 0.23 (\sin \alpha_e + \sin^{1/2} \alpha_e)\right] \text{ sec}$$

Azimuthal drift period, t_d

protons: $$\frac{5.65}{\gamma\beta^2 L} \frac{1.5}{(1 + 0.5 \sin \alpha_e)} \text{ sec}$$

electrons: $$\frac{1.04 \times 10^4}{\gamma\beta^2 L} \frac{1.5}{(1 + 0.5 \sin \alpha_e)} \text{ sec}$$

Occasionally it is desirable to follow a given particle's trajectory, i.e., in order to observe its exact penetration into the atmosphere. In such a thesis case, the dipole representation is sometimes too coarse.

* L denotes the magnetic shell parameter, equivalent to the geocentric distance of the line of force at the equatorial plane, in units of earth radii R. λ is magnetic latitude. α_e is the equatorial pitch angle.

The existence of a second adiabatic invariant, the longitudinal invariant, greatly relieves this problem. This quantity is:

$$I = \oint m\, v \cos \alpha \, dZ \qquad (15)$$

where

Z = path length of guiding center.

When variations of the field and effects of the drift remain small over one oscillation, Northrup and Teller (1960) have shown that I is conserved. Succeeding lines of force on which the particle may be found can then be predicted. Constancy of the magnetic moment allows equation (15) to be rewritten:

$$I = m\, v \oint \sqrt{1 - (B/B_m)}\, dZ \qquad (16)$$

As indicated previously, v is constant in a static magnetic field and therefore the invariant can be described in terms of the magnetic field only, without reference to any particular particle.

McIlwain (1961) developed a coordinate system based on the second invariant in order to organize measured data. Because the earth's field has anomolies which are fairly large, flux data plotted in dipole coordinates had appeared disordered. McIlwain describes magnetic shells, having the identification "L," on which the guiding center of a particle remains as it bounces and drifts. The value "L" is equivalent to the equatorial radius of the shell in a pure dipole field.

The field strength has been evaluated for a large number of lines (Jensen et al., 1960) using a spherical harmonic expansion of

the real field (Jensen and Whitaker 1960). Coupled with McIlwains's system, the results are a very useful set of tables, having utility in the analysis of the actual regions of penetration of the trapped radiation. These data were recently compiled in graphical form by Dudziak, Kleinecke and Kostigen 1963 . Their results are grouped into a number of sections. One section which is of particular utility to this work shows the topography of several magnetic shells between L = 1.0 and L = 6.0 and of magnetic field strength for altitudes from sea level to 2000 km. Another section shows the altitude variation of a number of locii of constant B and L values. One such curve is shown in Figure 26.

A third invariant, found by Northrup and Teller 1960 is the flux invariant

$$\phi = \int \vec{B} \cdot d\vec{A} \qquad (17)$$

The surface enclosing the flux is bounded by the mirror point traced around a complete azimuthal drift. The invariant flux is that which emerges from within this boundary. The invariant is conserved for field variations occurring over times considerably longer than the azimuthal drift period associated with any given particle under consideration.

B. Loss Processes and Lifetimes

The trapped radiation can be removed in any one of several ways. These are: (1) slowing down by gradual energy loss as in coulomb collisions, (2) catastrophic removal as in a nuclear collision wherein the

energy is lost all at once, (3) scattering out of the trapping region without losing much energy, and (4) failure of the trapping due to nonadiabatic effects. For protons, the chief natural method of removal is by gradual energy loss in collision with the constituents of the thin upper atmosphere, the exosphere. Electrons experience both slowing down and scattering.

Coulomb collisions cause a fast singly charged particle to lose energy at a rate of:

$$\frac{dE}{dt} = - 4\pi\, r_o^2\, mc^3\, \rho\, Z\, \Lambda/\beta \qquad (18)$$

where

$r_o = e^2/mc^2$ = classical electron radius

m = electron mass

ρ = number density (cm^{-3}) of absorber atoms or ions

Z = atomic number of absorber

Λ = log function related to nature of absorber.

This expression is valid for either protons or electrons if the slight difference in the log terms can be ignored. For neutral materials with an atomic ionization potential of I (Z),

$$\Lambda = \frac{1}{2}\left\{ \ell n \left[\frac{4\, m^2\, c^4\, \beta^4}{(1 - \beta^2)^2\, I^2\, (Z)} \right] - 2\, \beta^2 \right\} \qquad (19)$$

For fully ionized gases

$$\Lambda = \ell n\, (\lambda_D\, p/n) \qquad (20)$$

where

λ_D = Debye shielding distance

p = fast particle's momentum

For most cases under consideration $\Lambda \approx 23$ (Singer & Lenchek, 1962) in the hydrogen dominant exosphere. For other constituents, Λ is evaluated by replacing $\rho Z \Lambda$ by $\rho_E \times 23$. The value ρ_E is the equivalent electron density with respect to energy loss and may be obtained by multiplying ρ by the factor shown in Table II.

TABLE II
ATMOSPHERIC DENSITY CONVERSION

MULTIPLY TRUE DENSITY (cm^{-3}) BY THE APPROPRIATE CONVERSION FACTOR TO OBTAIN EFFECTIVE ENERGY LOSS DENSITY (ρ_E) OR SCATTERING DENSITY (ρ_S).

Material	Conversion Factor to ρ_E	Conversion Factor to ρ_S
Fully ionized hydrogen	1.0	2.0
Neutral hydrogen	0.47	0.4
Singly ionized oxygen	3.74	16.2
Neutral oxygen	3.22	14.4

Coulomb collisions produce a mean square deflection that accumulates at the rate of

$$\langle \Delta \theta^2 \rangle = 8\pi r_o^2 (m/m')^2 \rho Z^2 c \Lambda(1 - \beta^2)/\beta^3 \text{ rad}^2/\text{sec.} \quad (21)$$

where

m' = mass of the fast particle.

It is noted that scattering is more effective for electrons than for protons because of their smaller mass. The appropriate value of $\rho Z\Lambda$ can be obtained in a manner similar to that for energy loss except the correct factor is listed under ρ_S for scattering.

Energy loss and scattering in elastic nuclear collision are always negligible compared to coulomb collisions (Singer and Lenchek, 1962). Comparing nonelastic nuclear collisions with ionization loss, the time required for comparable energy loss gives an indication of their relative effectiveness. Integrating equation (18) between the limits of E_o, the initial energy, and E_o/e sets the lifetime for energy loss ($T_{1/e}$). This "lifetime" can be compared with the time required to reduce the number of fast particles to 1/e of its original value by catastrophic absorption:

$$T_{1/e}\,(\text{nucl}) = (\sigma_n\, \rho\, \beta c)^{-1} \qquad (22)$$

where

σ_n = nuclear cross section.

It can be shown for nonrelativistic particles, that the energy loss lifetime reduces to:

$$T_{1/e} = 6.7 \times 10^{10}\, E^{1.5}/\rho \text{ sec.} \qquad (23)$$

The particles are considered to be protons in fully-ionized hydrogen with density ρ ions cm^{-3} and E is expressed in MeV. This expression

is valid up to about 550 MeV in a hydrogen exosphere, after which nuclear collision becomes the predominant loss process. The proton lifetime is shown as a function of atmospheric density in Figure 4.

Similarly, a lifetime can be defined for electrons. For relativistic electrons the time required to slow down from β_1 to β_2 is (Singer and Lenchek, 1962):

$$T_E = \frac{g(\beta_1) - g(\beta_2)}{4\pi (e^4/m^2 c^4)\, c \wedge \bar{\rho}_E} \text{ sec.} \tag{24}$$

$$g(\beta) = \beta (1 - \beta^2)^{-1/2} - \arcsin \beta \tag{25}$$

The absorber density $\bar{\rho}_E$ is the average density over the path in equivalent electrons. Scattering competes with energy loss and is given by:

$$T_S = 1.5 \times 10^{12} \frac{\phi^2}{\rho_{SE}} \frac{\beta^3}{1 - \beta^2} \text{ sec.} \tag{26}$$

The concept of a lifetime is useful in determining the general behavior of a group of particles. The results of course must be interpreted in terms of the original definition of the lifetime. In this paper, lifetime will indicate reduction to $1/e^{th}$ of an original energy for energy loss by protons and a 90% energy loss, or scattering through approximately one radian, for electrons.

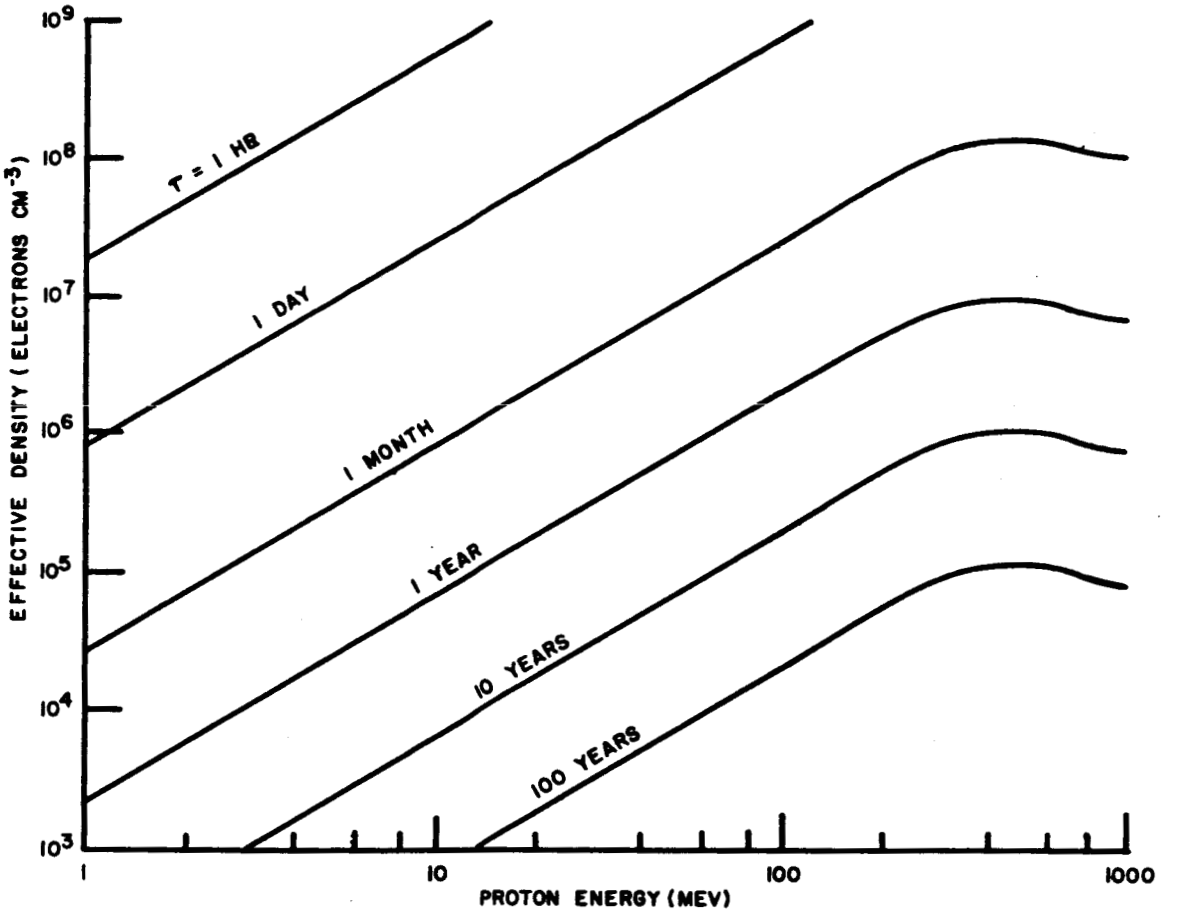

Figure 4. Proton Lifetimes

SECTION III

TIME DEPENDENCE OF THE RADIATION FLUX

In the study of the radiation belts the key ingredient in any set of experimental data is usually the integral or differential flux density. The flux levels are known to exhibit time variations. Since these time variations may be attributed to either the injection process or the removal process, or to both, it is essential that any fluctuations in the measured flux be explained in terms of a suitable model from among the many possibilities.

This section examines the simplified transport equation when suitable models of injection and removal are introduced. It is assumed that the natural injection function is approximately constant in the time scale of years. An impulsive injection represents the effect of introducing particles by artificial means, such as high altitude nuclear explosions. The removal process is described in turn by a number of models with varying dynamic properties, representing the natural effects of the atmosphere and its variations in density, or the possible effects of sweeper satellites. Hence, cases for various time dependent lifetimes are considered.

The basic equation which states the concentration of particles in a given region, the transport equation, can be stated as:

$$\frac{\partial n}{\partial t} + Kn = q_o \tag{27}$$

where

n = particle concentration, cm^{-3}

nK = loss rate, $cm^{-3}\ sec^{-1}$

q_o = injection rate $cm^{-3}\ sec^{-1}$

The loss factor K combines the effects of gradual energy loss, as in coulomb collisions, and of sudden loss as in nuclear collision or in collision with a thick absorber. The parameters n, K and q_o are not simply constants, but in fact are dependent on additional parameters such as energy, pitch angle, magnetic field strength and atmospheric density. In this section, only the time dependence will be treated in order that the time response of the concentration for given values of energy, magnetic field, etc. may be observed. The inverse of K, the particle "lifetime," is more commonly used.

A. Steady Injection

Assuming first that both the injection rate q_o and the life time $\tau = 1/K$ are constant in time, the most simple situation results:

$$n(t) = q_o \tau \left(1 - e^{-t/\tau}\right) + n_o e^{-t/\tau} \tag{28}$$

where

n_o = concentration at $t = 0$

$q_o\tau$ = final equilibrium concentration

This function is shown in Figure 5 where n_o has been set equal to zero. This situation would hold if it were assumed that at some time in history the radiation belts were void and then gradually filled to their final concentration according to the above expression.

B. Impulsive Injection

It is possible in present times to inject charged particles artificially into the earth's magnetic field. Such an event would impulsively change the concentration of particles in a given region of the magnetosphere. Specifically, the impulse is defined by

$$\text{Impulse} = \int q dt = Q\Delta t$$

$$= \Delta n_o$$

The change in concentration is Δn_o. Therefore this event can be represented by assigning a non zero value for Δn_o and assuming that q_o associated with this type of particle is either zero or has some other arbitrary constant value. Assuming the former, the concentration is given by:

$$n(t) = \Delta n_o \, e^{-t/\tau} \tag{29}$$

and is shown in Figure 6. If the equilibrium concentration of particles similar to those impulsively injected is not very much smaller than the impulsively injected ones, then they must be considered.

$$n(t) = q_o \tau \, (1 - e^{-t/\tau}) + (\Delta n_o + q_o \tau) \, e^{-t/\tau} \tag{30}$$

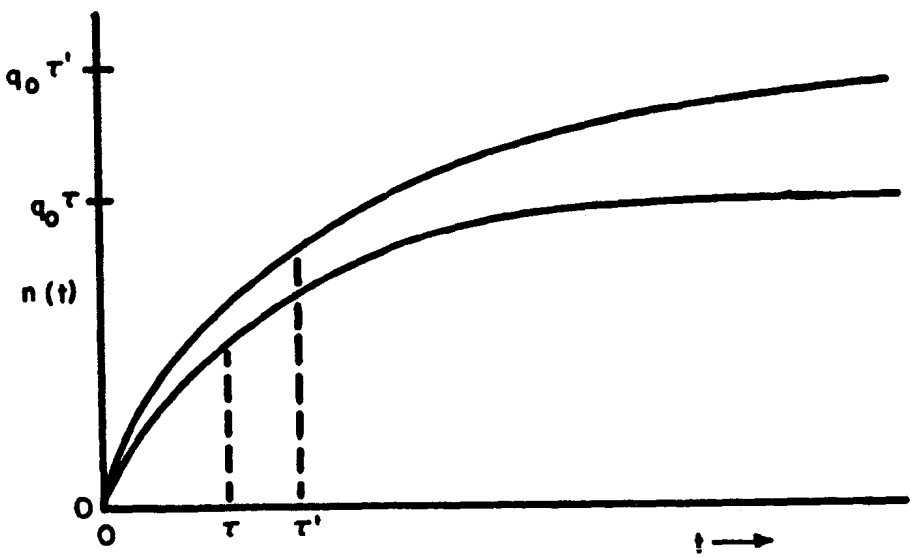

Figure 5. Particle Concentration With Steady Injection and Constant

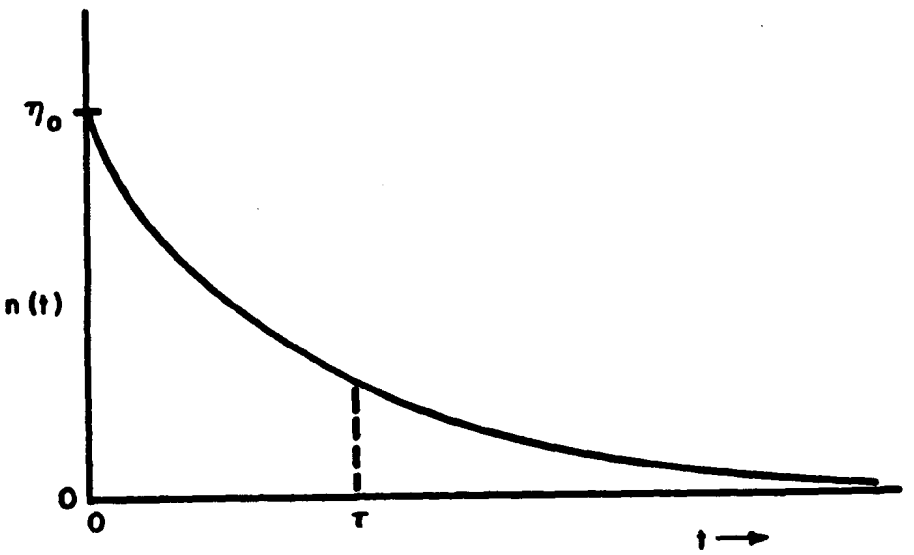

Figure 6. Particle Concentration With Impulsive Injection and Constant τ, Small n_o

This is shown in Figure 7 where Δn_o is arbitrarily chosen as 0.5 times $q_o \tau$.

This situation represents the recent case of the Starfish nuclear explosion above the Southern Pacific Ocean.

C. Impulsive Removal

Since the advent of the artificial satellite, the means are at hand for performing measurements on the radiation belts. It is also possible to inject a satellite of such dimensions that a region of the belts can be swept to a measureable extent. Such an event can be represented by a time dependent "lifetime" τ, where τ suddenly increases in magnitude in a given region.

It can be assumed that:

$$\tau\ (t < 0) = \tau_1$$

$$\tau\ (t > 0) = \tau_2 \ll \tau_1$$

and that the injection is steady, i.e. q_o = constant.

Therefore,

$$n(0) = n_o = q_o\ \tau_1 \tag{31}$$

and

$$n(t) = q_o\ \tau_2\ (1 - e^{-t/\tau_2}) + q_o\ \tau_1\ e^{-t/\tau_2} \tag{32}$$

This function is shown in Figure 8.

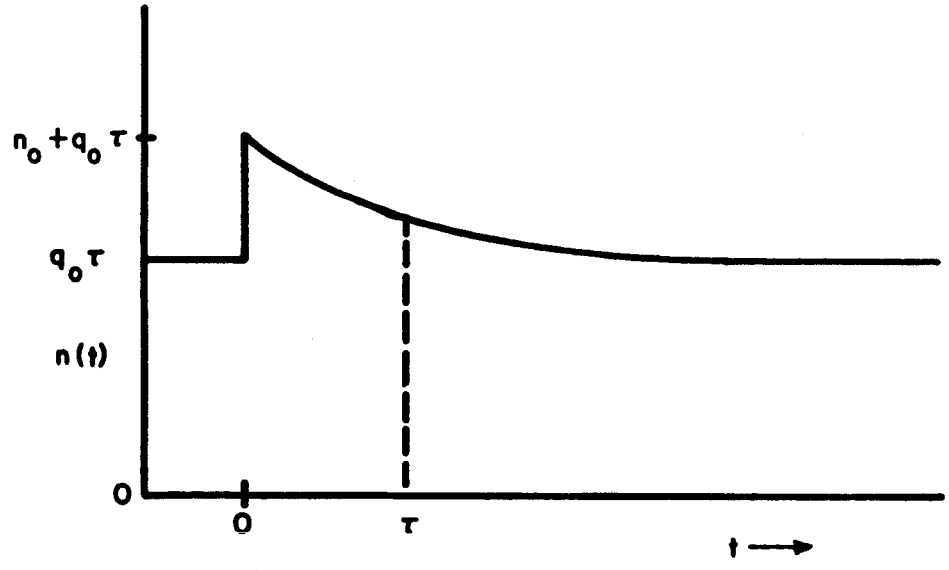

Figure 7. Particle Concentration With Impulsive Injection and Constant τ, Large n_o

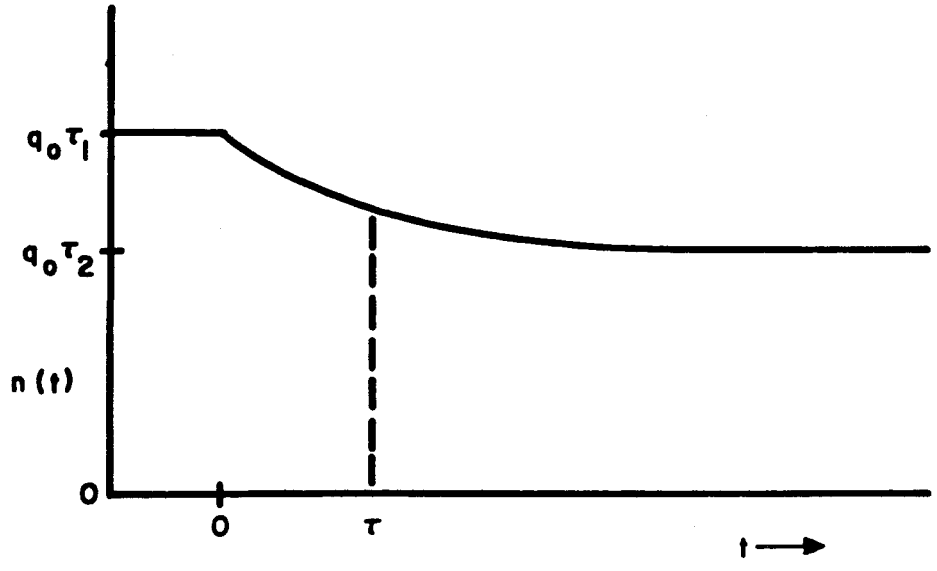

Figure 8. Particle Concentration With a Step Removal and Constant Injection

An extension of the principle of impulsive removal involves the assumption that the absorbing agent exists for a period of time that is on the order of the particle lifetime associated with the absorbing agent. In that case,

$$\tau\ (t < 0) = \tau_1$$

$$\tau\ (0 < t < t_1) = \tau_2$$

$$\tau\ (t > t_1) = \tau_1$$

and

$$n\ (0 < t < t_1) = q_o\ \tau_2\ (1 - e^{-t/\tau_2}) + q_o\ \tau_1\ e^{-t/\tau_2} \qquad (33)$$

$$n\ (t > t_1) = q_o\ \tau_1\ (1 - e^{-\frac{t - t_1}{\tau}}) + n\ (t_1)\ e^{-\frac{t - t_1}{\tau}} \qquad (34)$$

This is shown in Figure 9.

D. Steadily Increasing Removal

If it is assumed that the absorbing mechanism increases steadily in time, the resulting concentration will gradually diminish. Such a case might be an atmosphere with a density which increases according to

$$\rho\ (t\ ) = \rho_o + kt \qquad (35)$$

The particle lifetime as set by the atmospheric density would accordingly vary as:

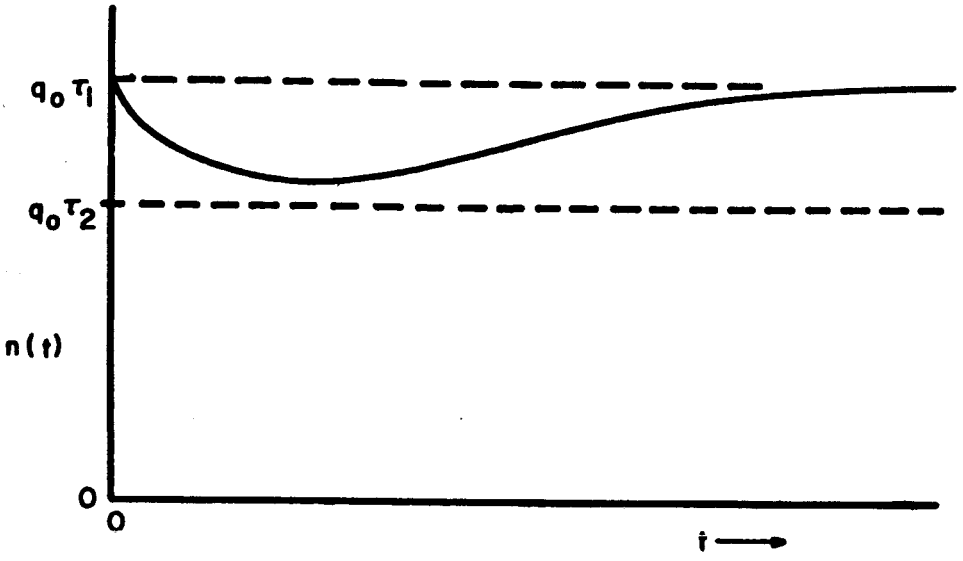

Figure 9. Particle Concentration With Impulsive Removal and Constant Injection

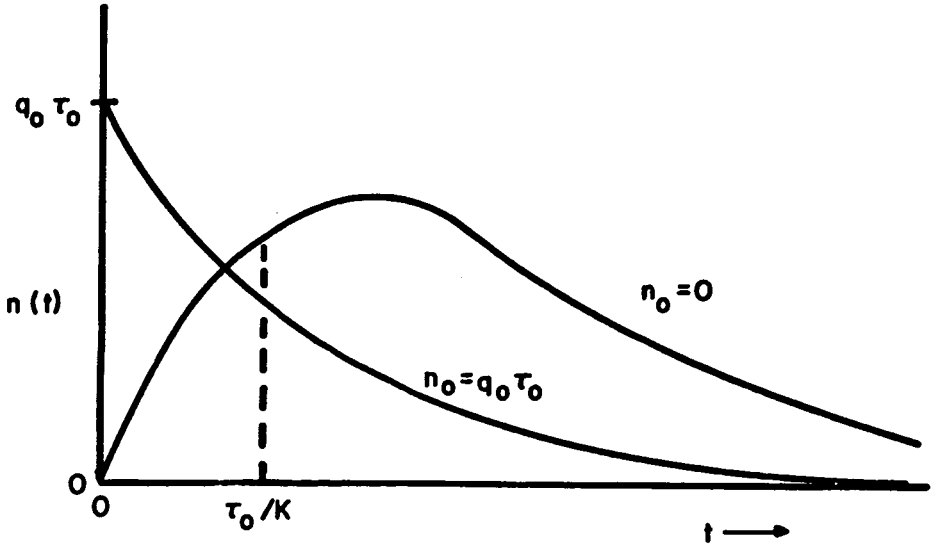

Figure 10. Particle Concentration With Steadily Increasing Removal and Constant Injection

$$\frac{\tau(t)}{\tau_o} = \frac{1}{1 + kt/\tau_o} \tag{36}$$

where k = rate at which τ changes from τ_o.

The resultant particle concentration would be given by:

$$n(t) = q_o \tau_o \left[\frac{1}{1 + \frac{kt}{2\tau_o}} - e^{-\frac{t}{\tau_o}\left[1 + \frac{kt}{2\tau_o}\right]} \right] + n_o e^{-\frac{t}{\tau_o}\left[1 + \frac{kt}{2\tau_o}\right]} \tag{37}$$

This function is shown in Figure 10 where n_o is assumed equal to zero in one case and equal to $q_o \tau_o$ in another case.

E. Continuously Varying Removal

The absorbtion mechanism may exhibit a time varying characteristic, such as might be caused by a fluctuating atmospheric density. The diurnal variation is one example. If it is assumed that the variation is simply sinusoidal, then the instantaneous density is given by

$$\rho = \rho_o (1 + \epsilon \sin \omega t). \tag{38}$$

Since the particle lifetime is inversely proportional to the atmospheric density, it follows that

$$\tau^{-1} = \tau_o^{-1} (1 + \epsilon \sin \omega t).$$

The resultant concentration is given by

$$n(t) = \frac{q_o \tau_o}{1+\frac{\epsilon}{\omega\tau_o}\left[(1-\cos\omega\tau_o)\ \cos\omega t + \sin\omega\tau_o \sin\omega t\right]}$$

$$+\left[n_o - \frac{q_o\tau_o}{1+\frac{\epsilon}{\omega\tau_o}(1-\cos\omega\tau_o)}\right] e^{-\frac{t}{\tau_o}\left[1+\frac{\epsilon}{\omega t}(1-\cos\omega t)\right]} \qquad (39)$$

It is immediately noted that the concentration is dependent on the time scale of the variation and the particle lifetime (i.e. on $\omega\tau_o$). For time scales which are relatively long compared to the particle lifetime, the effect of the modulation is attenuated. For short time scales, the concentration shows a significant cyclic variation. Figure 11 depicts the particle concentration when $\epsilon/\omega\tau_o$ is small. In Figure 12, $\epsilon/\omega\tau_o$ is much larger.

The case of atmospheric modulation of the particle flux and concentration is treated in greater detail in Section IV D.

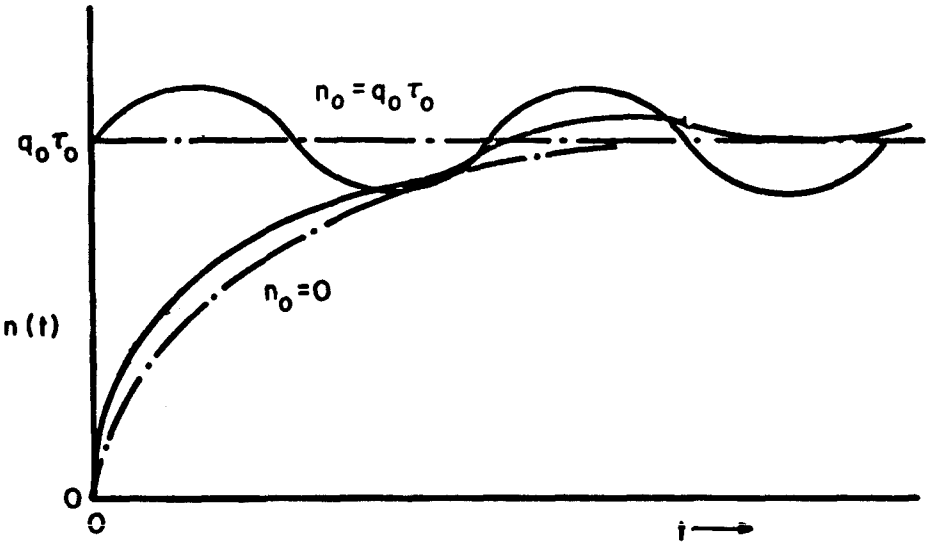

Figure 11. Particle Concentration With a Small Oscillating Removal and Constant Injection

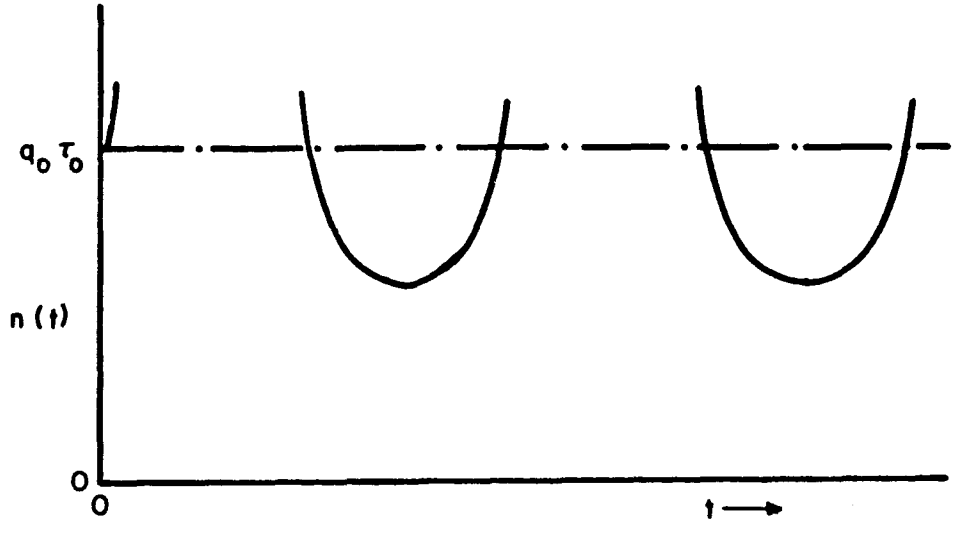

Figure 12. Particle Concentration With a Large Oscillating Removal and Constant Injection

SECTION IV

SPECIAL CASES

A. Sweeping of the Radiation Belt

The removal of particles by satellites sweeping through the radiation belts is characteristically different from that by the atmosphere. Since the atmosphere acts on all the particles in the radiation belt, the localized effect of a satellite appears as a perturbation of the total radiation. In this section, the extent of the sweeping action and the effect of a sweeper on particle lifetimes are discussed.

To begin with, the radiation lifetime can be derived from a consideration of the transport equation. Assuming an energy interval dE at E, the number of particles injected less the number removed per unit volume per unit solid angle per unit time, yields the net change in the concentration. The number injected depend on the injection function "q_o" and the number removed depend on the natural lifetime of the particles plus the number swept up by the satellite.

$$\therefore \Delta n = \text{no. injected} - \text{no. lost}$$

$$\text{no. injected} = q_o(E)\, dE\, dV\, d\Omega\, dt$$

$$\text{no. lost} = \left[n(E)\, dV\, d\Omega\, dE\right]\left[\tau(E)\right]^{-1} dt + j(E)\, dE\, d\Omega \left(\frac{d A_S}{dV}\right) dt\, dV \qquad (38)$$

where

$n(E)$ = concentration (cm^{-3} - $ster^{-1}$ - Mev^{-1})

q_o = injection rate (cm^{-3} - $ster^{-1}$ - Mev^{-1} - sec^{-1})

$\tau(E)$ = natural lifetime in exosphere (sec)

$j(E)$ = differential directional proton intensity (cm^{-2} - sec^{-1} - $ster^{-1}$)

$\frac{d A_S}{dV}$ = sweeper area per unit swept volume (cm^{-1})

But

$$j(E) = n(E) \cdot v = n(E) \beta c \tag{39}$$

$$\frac{dn(E)}{dt} = q_o - n(E) \left[\tau(E)^{-1} + \beta c \frac{d A_S}{dV} \right] \tag{40}$$

$$\frac{dn(E)}{dt} + \left[\tau(E)^{-1} + \beta c \frac{d A_S}{dV} \right] n(E) = q_o(E) \tag{41}$$

The solution of which is:

$$n = q_o/k + C_1 e^{-kt} \tag{42}$$

where

$$k = \left[\tau(E)^{-1} + \beta c \frac{d A_S}{dV} \right] \tag{43}$$

and

$$C_1 = n_o - q_o/k \quad \text{if } n = n_o \text{ at } t = 0$$

Therefore,

$$n = q_o/k \, (1 - e^{-kt}) + n_o e^{-kt} \tag{44}$$

It is seen that the contribution of the sweeper to the lifetime expression is

$$\tau_S = \left[\beta C \frac{d A_S}{dV}\right]^{-1} \tag{45}$$

The swept volume associated with this expression depends on the equatorial radius of the sweeper's orbit, assumed to be close to equatorial plane, the gyroradius of the swept particles and the depth of penetration of its guiding center along the line of force. As a first approximation this volume is given as (Singer, 1958 c):

$$dV \approx (2\pi r_e)\left(r_e \frac{H_o}{2r_e}\right)\left(\frac{Mc^2 \beta}{300B}\right)$$

$$= \frac{\pi r_e H_o Mc^2 \beta}{300B} \tag{46}$$

The units of Mc^2 are electron volts.

The depth of penetration has been limited by H_o, the atmospheric scale height. Particles penetrating past a scale height or so would have short lifetimes and would not be noticeably affected by the sweeper action. If a dipole approximation is assumed for the field, the equatorial value of the field strength is given by

$$B \approx 0.31 \left(\frac{R}{r_e}\right)^3 \tag{47}$$

$$\tau_S = \left\{\left[\frac{30C}{Mc^2 R}\right]\left(\frac{R}{r_e}\right)^4 \frac{A_S}{H_o}\right\}^{-1} \text{ sec.} \tag{48}$$

It is interesting to note that (1) this lifetime is independent of the particle energy (as one would expect since catastrophic absorption was implicitly assumed) and (2) the lifetime increases with the fourth power of "R." It is of further interest to note that the extent of the swept region, being energy dependent, covers a radial range given by the following.

$$\text{Radial Range} \approx \frac{Mc^2\beta}{300B} = \frac{Mc^2\beta}{93}\left(\frac{r_e}{R}\right)^3 \sim E^{1/2} \text{ for } \beta \ll 1 \quad (49)$$

For

$$\left(\frac{r_e}{R}\right)^3 = (1.2)^3 \approx 1.8$$

and

$\beta \approx 0.5$, the radial range $\approx 10^7$ cm.

This represents 2% of R, the earth's radius, where $R \approx 6 \times 10^8$ cm. Therefore, high energy protons can be swept over distances which are modest but not altogether insignificant with respect to the extent of the inner zone by a single sweeper.

Evaluating the sweeper time constant, if it is assumed that $H_o \approx 200$ km at 1000 km altitude, and A_S is expressed in cm^2, then

$$\tau_S = 1.04 \times 10^{13} \frac{1}{A_S}\left(\frac{r_e}{R}\right)^4 \approx 2 \times 10^{13}/A_S \text{ sec.} \quad (50)$$

The proton lifetime in the swept environment is compared to the lifetime as set by the atmosphere in Figure 13. It is noted that reasonably

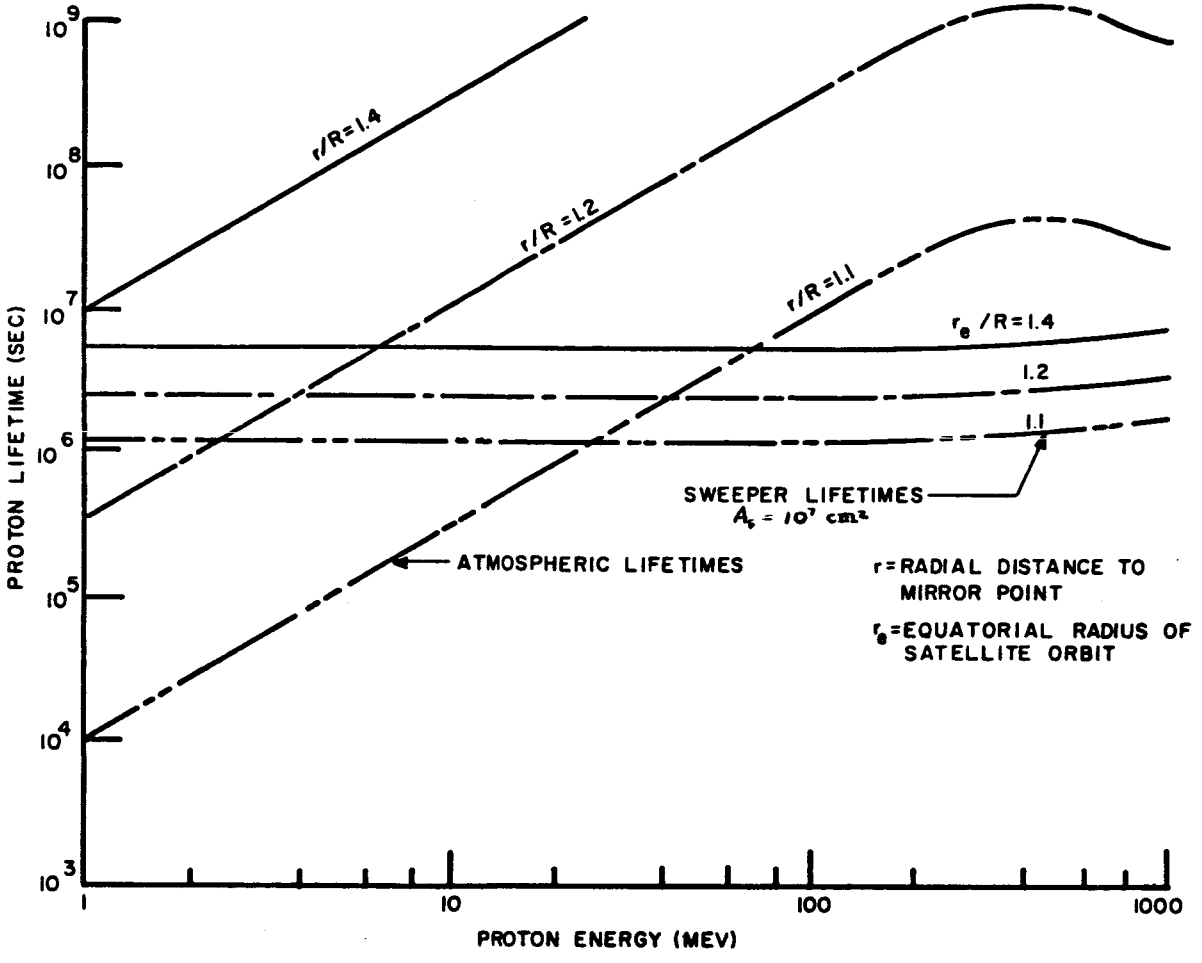

Figure 13. Proton Lifetimes as Limited by Energy Loss in the Atmosphere and by the Effect of a Sweeper Satellite

sized sweeper areas can compete with atmospheric processes at energies of several hundred Mev.

Since, in general however, a sweeper satellite may not traverse a circular orbit which is concentric with the orbit of geomagnetically trapped particles as assumed in the previous paragraphs, such a satellite would not be expected to sweep a given region continuously. Rather, a relative radial motion would exist wherein the sweeper spent only part of its orbital period in a given radial region. Such a case was developed by Singer (1962b) in connection with a circular satellite orbit in an eccentric dipole field. The net result of this effect is to reduce the effective sweeper area by some fraction, thereby modifying the sweeping rate in any one region. At the same time, the sweeper penetrates into deeper regions.

The following describes the effective sweeper area in terms of the geometric parameters. Let it be assumed that a planet's mass center and its magnetic dipole center are displaced by a distance Δ. A sweeper at an orbital radius R_S would appear to traverse a path in the geomagnetic coordinates given approximately by:

$$R_S' \approx R_S + \Delta \sin \omega_S t \qquad (51)$$

A trapped particle at a mean equatorial radius r_e will intersect the geomagnetic equatorial plane within a region defined by the radial limits $(r_e + a)$ and $(r_e - a)$ where "a" is the Larmor or gyroradius for the particle. As shown in Figure 14, the orbital path of the sweeper will

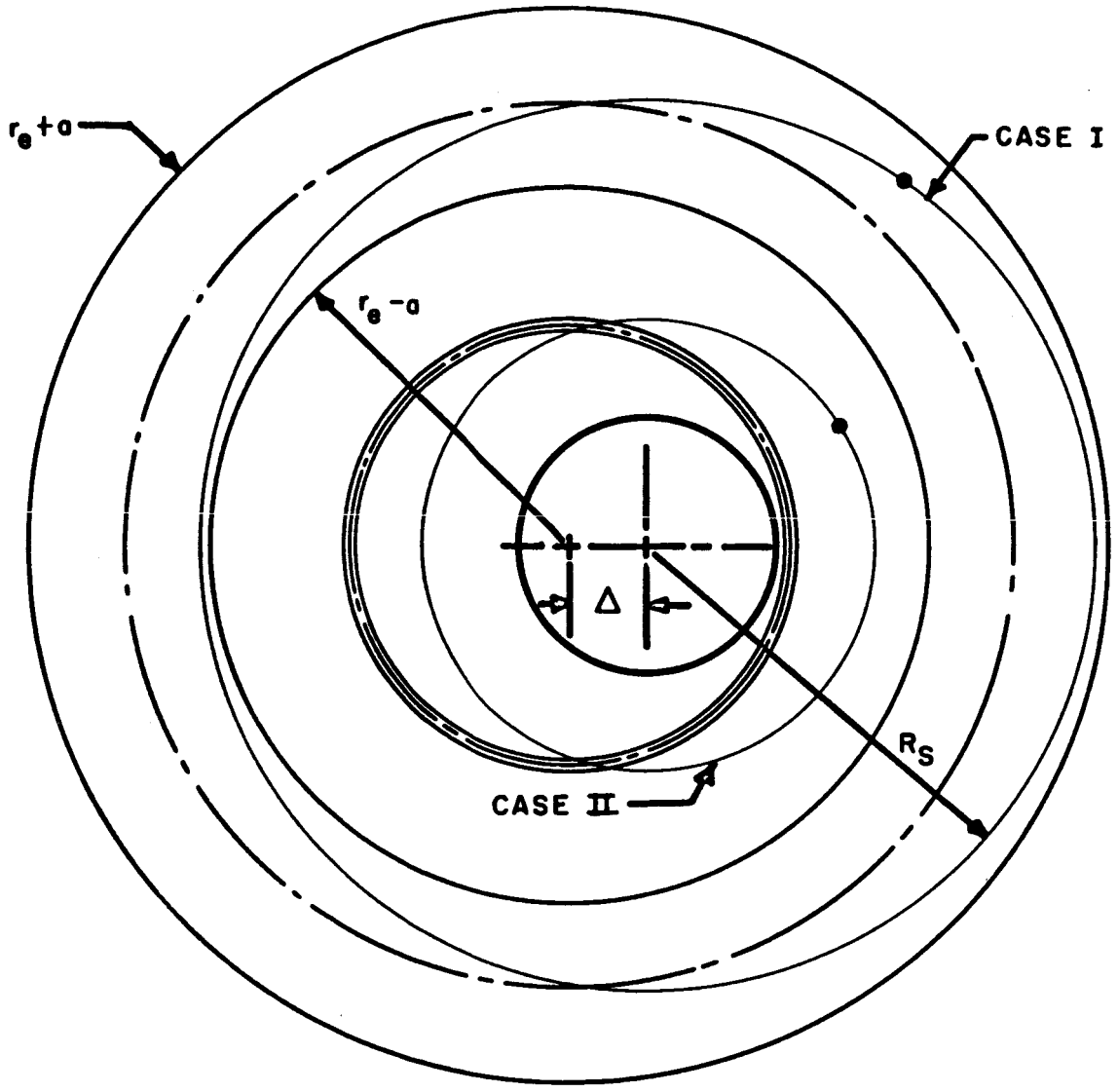

Figure 14. Satellite Orbit and Particle Orbit in an Eccentric Magnetic Field

intersect this region at θ_{max} and θ_{min}. It is assumed that the sweeper orbit is nominally in the same plane as the magnetic equatorial plane.

The probability that the trapped particle will collide with the sweeper is simply the ratio of the effective sweeper area to the allowed equatorial area for the particle. The latter is:

$$(2\pi r_e)(2a) = 4\pi r_e a \tag{52}$$

The effective area of the sweeper is proportional to the time spent by the sweeper within the radial region $(r_e + a)$ to $(r_e - a)$. Referring to Figure 14 and using the law of cosines,

$$(r_e \pm a)^2 = R_S^2 + \Delta^2 - 2R_S \Delta \cos\theta \tag{53}$$

$$\theta_{max} = \arccos\left[\frac{1}{2R_S \Delta}\left(R_S^2 + \Delta^2 - (r_e + a)^2\right)\right] \tag{54}$$

$$\theta_{min} = \arccos\left[\frac{1}{2R_S \Delta}\left(R_S^2 + \Delta^2 - (r_e - a)^2\right)\right] \tag{55}$$

and

$$t/\tau = (\theta_{max} - \theta_{min})/\pi \tag{56}$$

For

$$\theta_{max} = \theta + \epsilon_1 \text{ and } \theta_{min} = \theta - \epsilon_2,$$

where it is assumed that ϵ_1 and ϵ_2 are small, the difference $(\theta_{max} - \theta_{min})$ can be solved utilizing

$$\cos(\theta + \epsilon_1) = \cos\theta \cos\epsilon_1 - \sin\epsilon_1 \sin\theta$$

$$\approx \cos\theta \cos\epsilon_1 - \epsilon_1 \sin\theta \tag{57}$$

$$\cos(\theta - \epsilon_2) = \cos\theta \cos\epsilon_2 + \sin\epsilon_2 \sin\theta$$

$$\approx \cos\theta \cos\epsilon_2 + \epsilon_2 \sin\theta \tag{58}$$

where

$$\theta_{max} - \theta_{min} = \epsilon_1 + \epsilon_2 = \frac{\cos\theta_{min} - \cos\theta_{max}}{\sin\theta} \tag{59}$$

$$= \frac{1}{2R_S \Delta \sin\theta}\left[(R_S^2 + \Delta^2 - (r_e - a)^2) - (R_S^2 + \Delta^2 - (r_e + a)^2)\right] \tag{60}$$

$$= \frac{2a\, r_e}{R_S \Delta \sin\theta} . \tag{61}$$

But

$$\sin\theta = \left[4 R_S^2 \Delta^2 - (R_S^2 + \Delta^2 - r_e^2)^2\right]^{1/2} / 2R_S \Delta \tag{62}$$

and

$$\therefore t/\tau = \frac{1}{\pi}\left\{(\frac{2a}{\Delta})(\frac{r_e}{R_S})\left[1 - \left(\frac{R_S^2 + \Delta^2 - r_e^2}{2R_s \Delta}\right)^2\right]^{-1/2}\right\} \tag{63}$$

The net probability of a collision is therefore,

$$P = \frac{A_{eff}}{4\pi r_e a} = \frac{A_S \frac{\delta\theta}{\pi}}{4\pi r_e a}$$

$$= \frac{A_S}{2\pi^2 R_S \Delta}\left[1 - \left(\frac{R_S^2 + \Delta^2 - r_e^2}{2R_S \Delta}\right)^2\right]^{-1/2} \tag{64}$$

Since a collision will catastrophically absorb a trapped particle (e.g., a proton), the lifetime of a given particle is determined by the bounce period and the probability for a collision with the sweeper. Hence the equivalent lifetime of a proton in a swept environment is given by:

$$\tau_S = \frac{1}{2} T_{NS}/P$$

where

$$T_{NS} \approx \left[1.38 - 0.32 \left(\sin^{1/2} \alpha_e + \sin \alpha_e\right)\right] \frac{2 r_e}{\beta c} \qquad (65)$$

It is interesting to note that the proton lifetime under the circumstances set forth appears to be energy dependent due to the factor β^{-1}. The reason for this is that the probability function is independent of the gyroradius and hence β, whereas the bounce time is not. The probability function becomes dependent on the gyroradius when the included angle $\theta_{max} - \theta_{min}$ is no longer small and sin ϵ cannot be approximated by ϵ. This occurs when sin θ becomes smaller than several times $(\frac{a}{\Delta})$. This condition is identical to:

$$1 - \frac{\left(R_S^2 + \Delta^2 - r_e^2\right)^2}{4 R_S^2 \Delta^2} \lesssim \left(\frac{a}{\Delta}\right)^2 \qquad (66)$$

Therefore, when $\Delta \approx 0$ for instance, the probability function must be restated as

$$P = \frac{A_S(\delta\theta)}{4\pi^2 r_e a} \qquad 0 \ll \delta\theta \leq \pi \qquad (67)$$

Since the gyroradius is energy dependent, i.e.

$$a = \frac{Mc^2 \beta \gamma}{300B} , \tag{68}$$

the proton lieftime is seen to be independent of energy for $\beta << 1$:

$$\tau_S = \frac{r_e}{\beta c} \frac{4\pi^2 r_e}{A_S(\delta\theta)} \frac{Mc^2 \beta}{300B}$$

$$= \frac{4\pi^2 r_e^2 Mc^2 \gamma}{300c\ B\ A_S(\delta\theta)} ; \tag{69}$$

$$\therefore \tau_S = \frac{4\pi^2}{93} \frac{Mc^2 r_e^5 \gamma}{cR^3 A_S(\delta\theta)}$$

$$= 1.6 \times 10^{26} \left(\frac{r_e}{R}\right)^5 \frac{1}{A_S(\delta\theta)} \tag{70}$$

For low altitudes and $\delta\theta = \pi$, the proton lifetime is about $0.5 \times 10^{26}/A_S$ seconds. This is considerably greater than the lifetime previously estimated. The difference arises from the containing volume associated with the trapped particles. In the first approach, this volume was determined from the atmospheric scale height and the equatorial area. In the present derivation, the extent of the bounce path implied in the bounce period and the equatorial area were used.

Particle lifetimes are therefore summarized as:

$$\tau_S = 4\pi^2 R_S r_e \Delta \left[1 - \frac{(R_S + \Delta^2 - r_e^2)^2}{r R_S^2 \Delta^2}\right]^{1/2} / A_S \beta c \quad \text{for } \frac{\Delta}{R} >> 0 \tag{71}$$

$$\tau_S = \frac{4\pi^2}{45} \frac{Mc^2 \gamma R^2}{c} \left(\frac{r_e}{R}\right)^5 \frac{1}{A_S(\delta\theta)} \quad \text{for } \Delta \approx 0;\ 0 << \delta\theta \leq \pi \tag{72}$$

In the case of the earth, the magnetic dipole is displaced from the geographic axis by:

$$\Delta = 430 \text{ KM} = .063 \text{ R}$$

For $\beta \approx .5$ and $r_e/R = 1.2$, the lifetime is calculated from (71) to be

$$\tau_S = 6.3 \times 10^{16}/A_S \text{ seconds.}$$

For a one year proton lifetime, it is required that A_S be on the order of 2×10^5 m^2.

The geometrical conditions which give rise to the predominance of either the energy dependent or energy independent lifetimes may be generalized by referring to Figure 14. The energy dependent lifetime holds when $(\delta\theta)$ is very small, as in case II. The energy independent lifetime holds when $(\delta\theta)$ is large, as in case I. The conditions which allow types like case II to occur are large values of Δ and small values of a, r_e and R_S. For either smaller values of Δ or larger values of a, r_e, and R_S, the eccentricity becomes less effective and the energy independent case I predominates. Assuming a hypothetical case where $\Delta = 0.2\ R_e$, the lifetimes of particles in the swept environment for the above two cases are given in Table III.

TABLE III

PROTON LIFETIMES IN A SWEPT ENVIRONMENT
$A_S \tau_S$ (cm^2 -sec.)

	Case I ($\delta\theta = \pi$)	Case II ($\Delta = 2.R$)	
r_e/R		$\beta = .5$	$\beta = .25$
1.2	0.9×10^{26}	2.6×10^{17}	5.2×10^{17}
1.5	2.6×10^{26}	4.1×10^{17}	8.2×10^{17}
2.0	1.1×10^{27}	7.3×10^{17}	1.5×10^{18}

B. Interpretation of the "Hole" in the Radiation Belt

It has been shown in the previous section that a satellite sweeping through the radiation belts absorbs particles and thereby modifies the measured flux level in that region. Upon close examination of the flux profile, it is found that a number of physical characteristics pertaining to the radiation, the magnetic field, the atmosphere, and the sweeper can be deduced from omnidirectional differential (in energy) flux measurements as a function of distance. These include the following:

	Reference Eqn.
A. Magnetic Field Properties	
1. Field strength (B)	93
2. Displacement of the planet's magnetic dipole from the planetary center (Δ)	84
B. Radiation Belts	
1. Injection rate of the particles (q_o)	96
2. Particle energy (E)	-

3. Particle speed (βc) -

4. Particle lifetime (τ) 72, 78, 82

5. Gyroradius (a) -

C. Atmosphere

1. Density (ρ) 98

D. Sweeper Satellite

1. Sweeper area (A_S) 88

Evaluation of the above parameters proceeds as follows. It is assumed that a region containing trapped radiation is swept by a sweeper satellite, either natural or artifical. An instrument probe, crossing the path of the sweeper measures the flux intensity j(E) of the radiation belt over a wide range of energies (E). Such a set of data would appear as shown in Figure 15, where the measured flux intensity has been converted to concentration according to:

$$n = j(E)/v(E)$$

where

v = particle velocity.

General properties of the flux or concentration measurements

The maximum value of the flux, and therefore the concentration, is set by atmospheric properties in regions distant from the sweeper. As the sweeper path is approached, more and more of the trapped particles traverse orbits which cross the sweeper's path and therefore can be absorbed. The intensity accordingly drops off. The minimum value

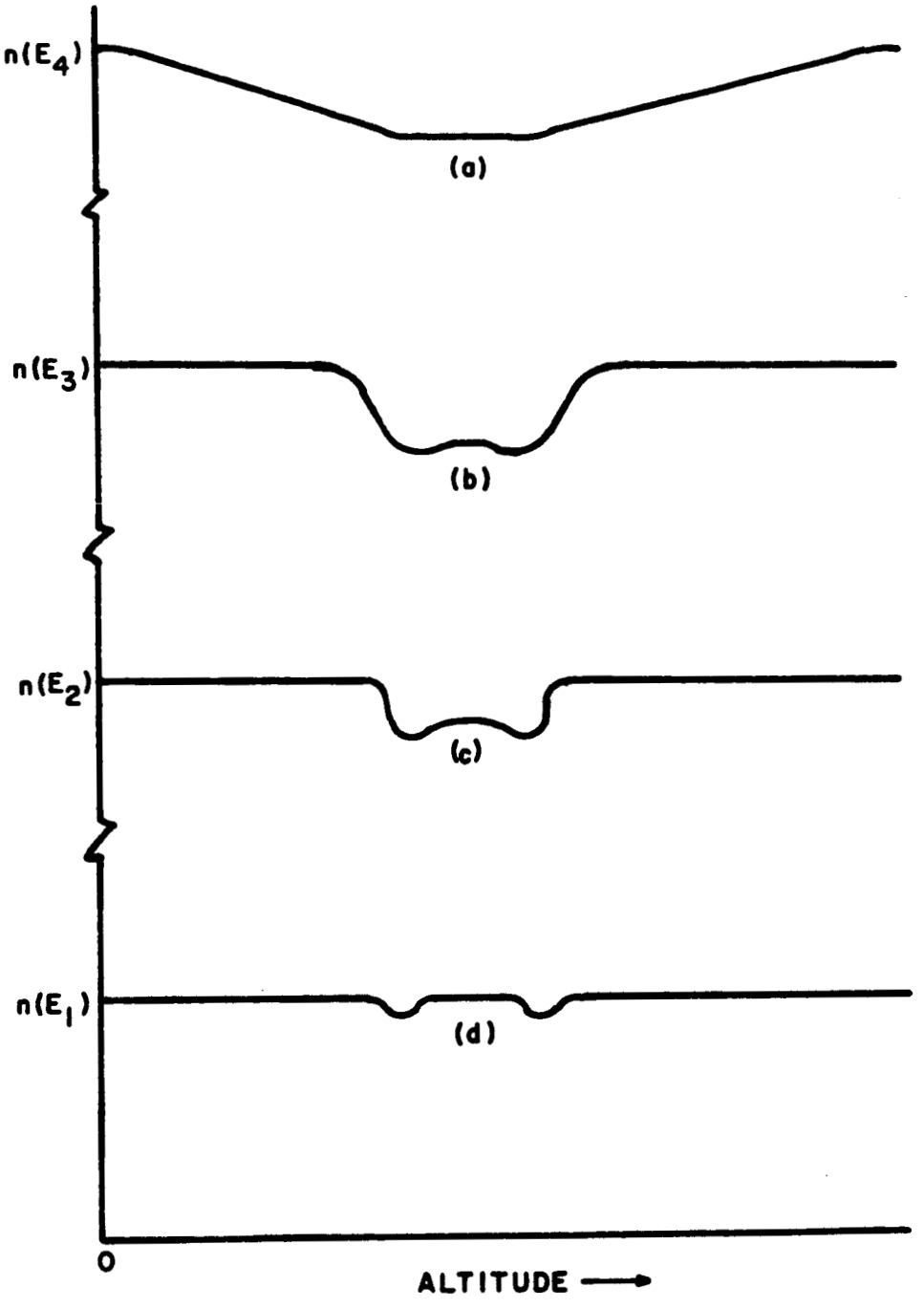

Figure 15. Particle Concentrations in the Vicinity of a Swept Region

is set by the sweeper area and properties of the particles and orbits. For values of $\Delta>0$, and for a $<<\Delta$, the sweeper spends varying amounts of time in different parts of the swept region. The width of the swept region is Δ + d, where d is the width or diameter of the sweeper. Since the sweeper spends more time near the edges of the swept band than near the center, the sweeper is more effective at the edges and the intensity at the edge is accordingly lowest. Therefore a difference in intensity is expected between the edge and the center, as shown in Figure 15-c. For higher energies however, the gyroradius increases and tends to smooth the intensity curve as shown in Figure 15-b and 15-a. The intensity is also energy dependent for a $<<\Delta$. Therefore the minimum value decreases for higher energies. Conversely, the minimum values increase for lower energies until, especially at the center of the swept band, the flux intensity approaches the limit set by the atmosphere. This is shown in Figure 15-d.

For very small values of "Δ", the intensity profile approaches that of Figure 15-a where a relative maximum at the center of the swept region is no longer discernible.

Determination of gyroradius "a"

Re-examining Figure 15, the gyroradius for any given energy E can be observed directly from the flux profile. The gyroradius is simply half the distance between the locations corresponding to the minimum flux and the flux set by the atmosphere. This can be seen by noting

the following. At the edge of the swept region, assuming an isotropic velocity distribution, a particle of gyroradius "a" with velocity vector $\vec{v}$ pointing in any direction passes into the swept region. Half of the particles at X = a enter the swept region and a particle at 2a just grazes the swept region. The fraction depends on X and a and is given by $\frac{\alpha}{\pi}$. From Figure 16 the geometry indicates that:

$$\alpha = \arccos\left(\frac{X}{a} - 1\right). \tag{73}$$

The resultant profile of the fraction absorbed versus the separation of the measuring instruments from the edge of the swept region is shown in Figure 17. Hence, the gyroradius of particles of a given energy interval can be taken directly from the flux profile data for that energy interval.

Determination of the eccentricity (Δ) of the magnetic dipole field

If data of the type shown in Figure 15-b, c and d, is obtained, it is clearly evident that either the magnetic field is offset from the geocenter, which controls the motion of the sweeper, or the sweeper orbit is noncircular. If this latter effect is measurable, it can be deducted from the gross offset, yielding the magnetic offset. For suitably small values of "a", the data reveals "Δ + d" directly where "d" is the diameter of the sweeper. This is shown in Figure 18. If "d" is known to be much smaller than Δ, then Δ is obtained directly.

As a cross check to this method, the flux intensities at different parts of the swept region can be used to determine Δ.

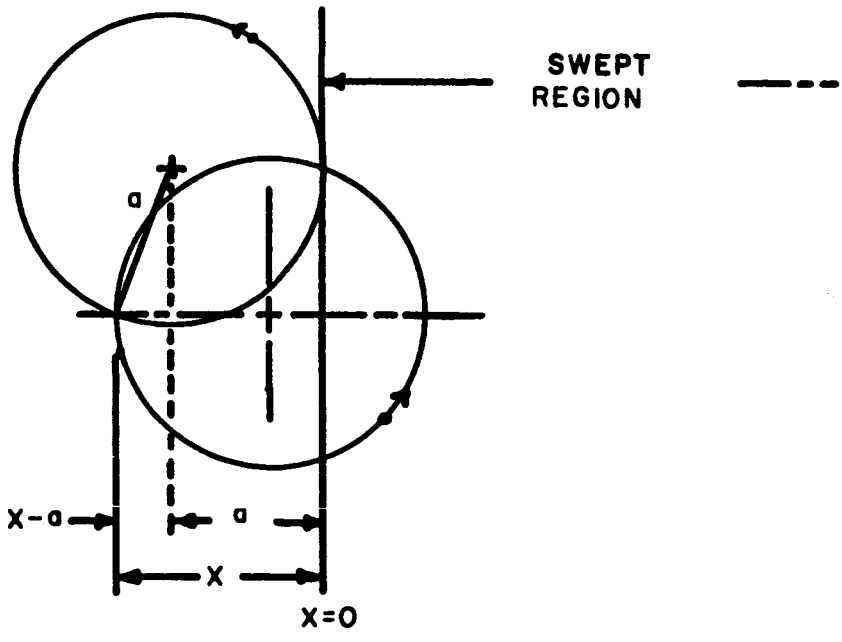

Figure 16. Particle Orbit Intersecting Swept Region

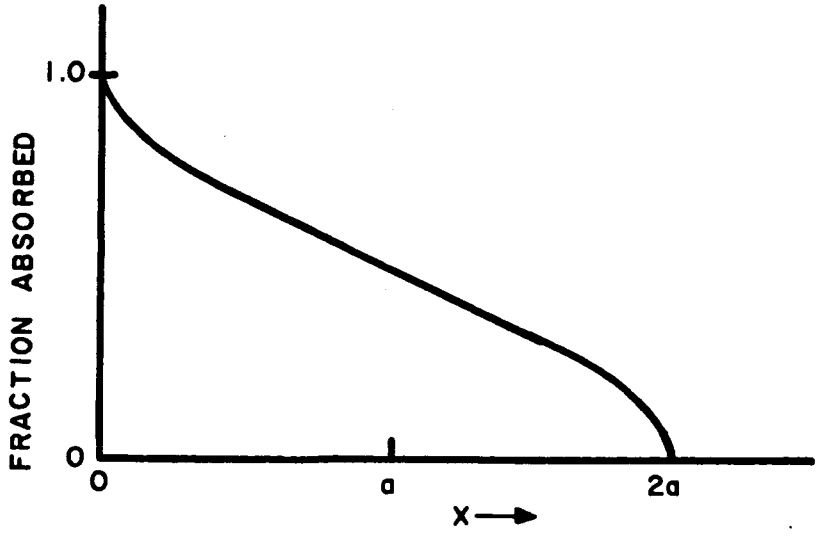

Figure 17. Absorption Fraction vs Separation From Swept Region

As derived in the previous section, the particle lifetime in a swept environment is:

$$\tau_S = \frac{\frac{1}{2} T_{NS}}{P} = \frac{r_e}{\beta c} \Big/ \frac{A_S(\delta\theta/\pi)}{4\pi r_e a}$$

$$= \frac{4\pi^2 r_e^2 a}{A_S \beta c (\delta\theta)} \tag{74}$$

For "a" sufficiently small, $\delta\theta$ can be approximated and τ_S solved. The gyroradius "a" is considered small when $a \ll \Delta$. This can be judged by observing the data or by noting the energy dependence of the flux measurements. For $a \ll \Delta$, τ_S is independent of energy, hence of β. For $a \sim \Delta$, τ_S varies as $1/\beta$. A comparison of flux data at several energy levels allows the proper data to be selected. Normalized to the spectrum of protons with lifetimes set by exospheric absorption, the transition from an energy dependent sweeping to an energy independent sweeping is recognized from the following. For $j_{atmos}/j_{sweeper} \sim E^{1.75}$ to $E^{2.5}$, the gyroradius is small. For this ratio $\sim E^{1.5}$, the gyroradius is large. Having chosen the proper energy level, namely a small one, the flux at the edge of the swept region is compared to the flux at the center of the band for the same energy interval.

$$j(E) = n(E)\ v(E) = v(E)\ q_o(E)\ \tau_S(E) \tag{75}$$

$$\frac{j_{center}}{j_{edge}} = \frac{\tau_S\ center}{\tau_S\ edge} \tag{76}$$

For "a" $\ll \Delta$,

$$\delta\theta = \frac{2a\, r_e}{R_S \sin\theta} \tag{77}$$

At the center of the swept region $\sin\theta \approx 1.0$

$$\tau_S = \frac{4\pi^2 r_e R_S \Delta}{A_S \beta c} \tag{78}$$

At the edge of the band,

$$\delta\theta = \theta_{max} \approx \arccos \frac{R_S - 2a}{R_S} \tag{79}$$

$$\cos\theta \approx 1 - \frac{\theta^2}{2} = 1 - 2\frac{a}{R_S} \tag{80}$$

$$\text{and } \therefore \delta\theta \approx 2\sqrt{\frac{a}{R_S}} \tag{81}$$

$$\tau_S = \frac{4\pi^2 r_e}{A_S c}\sqrt{a R_S} \tag{82}$$

with the result that

$$\frac{j_{center}}{j_{edge}} = \frac{\Delta\sqrt{R_S}}{r_e\sqrt{a}} \tag{83}$$

$$\therefore \Delta = \frac{r_e\sqrt{a/R_S}}{\left(\frac{j_{center}}{j_{edge}}\right)} \tag{84}$$

If the outer edge is used,

$$r_e + a = R_S + \Delta \tag{85}$$

If the inner edge is used,

$$r_e - a = R_S - \Delta \tag{86}$$

In most cases $R_S \approx r_e$.

Knowing R_S or r_e, substitution into these equations reveals the value of Δ.

Determination of the sweeper dimensions (d and A_S)

For values of 2a less than the diameter of the sweeper (d), the actual cross section for collision is no longer $A_S = \frac{\pi}{4} d^2$ but is given by $A_S\,(2a < d) = 2ad$.

For measurements of flux near either the edge or center of the band,

$$\frac{j\,(2a < d)}{j\,(2a > d)} = \frac{A_S(2a > d)}{A_S(2a < d)} \cdot \frac{q_o(2a < d)}{q_o(2a > d)} = \frac{(\pi/4)\,d^2}{2ad} \cdot \frac{q_o(2a < d)}{q_o(2a > d)} \tag{87}$$

$$\therefore d = \frac{8}{\pi} a \frac{j\,(a)}{j\,(a')} \frac{q_o\,(a')}{q_o(a)} \tag{88}$$

where

$a < d/2$ and $a' > d/2$.

The problem of determining which values of "a" are larger than "d/2" and which values are smaller than d/2 and what values of q_o to use is not difficult. After the least acceptable value of a' is determined, it is assumed $q_o(a') \approx q_o(a)$ and "d" is solved for several values of j(a'). Extrapolation to the limit j(a) yields the correct value of "d". The least acceptable value of "a'" and the proper value of "a" are determined by scanning the flux in the swept region across the energy spectrum and

comparing with a similar scan in an area removed from the swept region. It is assumed that the injection q_o does not vary significantly over about two gyroradii. It is remembered that the particle lifetimes in the swept environment near the edge of the band and near the center of the band are:

$$\tau_S = \frac{4\pi^2 r_e^2}{A_S \beta c} \sqrt{a R_S} \tag{82}$$

and

$$\tau_S = \frac{4\pi^2 r_e R_S \Delta}{A_S \beta c} \tag{78}$$

respectively. Substituting first $A_S = \frac{\pi}{4} d^2$ for $2a > d$ and then $A_S = 2ad$ for $2a < d$, it is found that:

$$\tau_S (2a < d) \sim \beta^{-3/2} \qquad \text{(near the edge of the band)} \tag{89}$$

$$\tau_S (2a < d) \sim \beta^{-2} \qquad \text{(near the center of the band)} \tag{90}$$

$$\tau_S (2a > d) \sim \beta^{-1/2} \qquad \text{(near the edge)} \tag{91}$$

$$\tau_S (2a > d) \sim \beta^{-1} \qquad \text{(near the center)} \tag{92}$$

When the flux in the swept region is compared to the flux away from the swept region, where atmospheric loss is the controlling factor, the relative spectra change near $2a = d$. The results are indicated in Table IV and Figure 19.

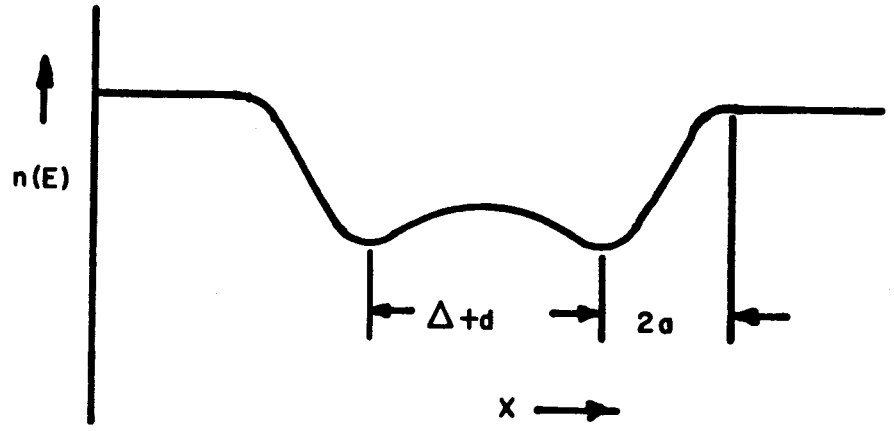

Figure 18. Detail of Flux Profile

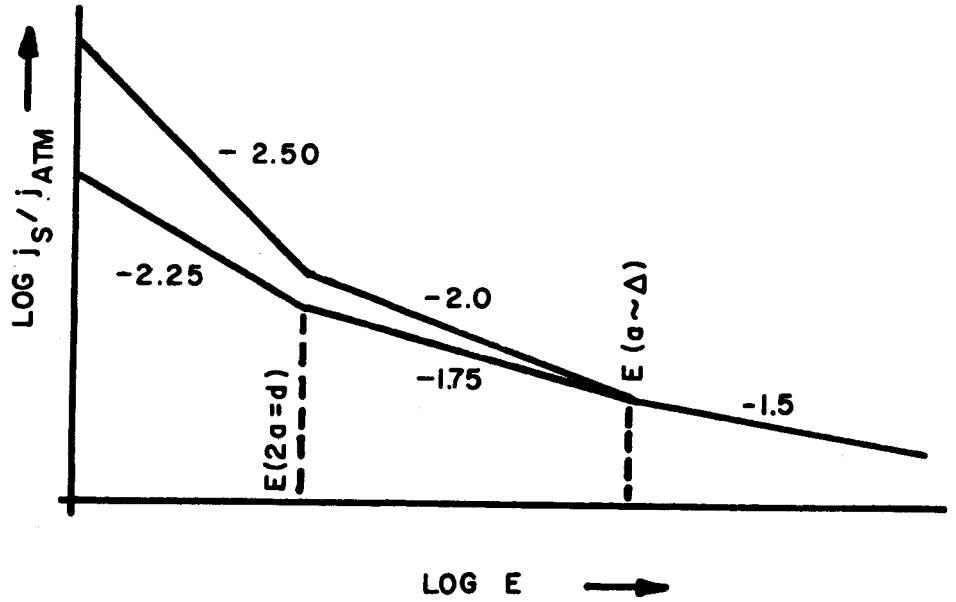

Figure 19. Sweeper Limited Flux: Atmospheric Limited Flux vs Energy

TABLE IV

ENERGY DEPENDENCE OF $j_s/j_{atm} \sim E^n$

	$a(E) < d/2$	$d/2 < a(E) < \Delta$	$a(E) > \Delta$
n*	-2.5	-2.0	-1.5
n**	-2.25	-1.75	-1.5

n* is n when j_s is measured near the center of the swept band.

n** is n when j_s is measured near the edge of the swept band.

The proper value of j(a) corresponds to j_s of $j_s/j_{atm} \sim \beta^{-2.5}$ or $\beta^{-2.25}$. The proper value of j(a') corresponds to j_s of $j_s/j_{atm} \sim \beta^{-1.5}$ to $\beta^{-2.0}$.

If the magnetic field strength were known, the gyroradius "a" as a function of energy would be known. The intersection of the slopes -2.5 and -2.0 or of the slopes -2.25 and -1.75 for the flux-energy spectrum would also indicate the sweeper dimension, since if "a" at this intersection was determined, it would follow that d = 2a. Assuming that the sweeper is a spheroid, the sweeper cross section is simply $A_S = \frac{\pi}{4} d^2$.

Determination of magnetic field strength (B)

The gyroradius "a" of a charged particle in a magnetic field is given by

$$a = \frac{Mc^2 \beta \gamma}{300B} \text{ (cm)} \qquad (68)$$

An instrumented proble, detecting particle fluxes would be able to determine $\beta\gamma$ for a given narrow band of energies. Examination of the flux profile would reveal the gyroradius, according to the methods of previous paragraphs. Solution of the value of B follows directly:

$$B = \frac{Mc^2 \beta\gamma}{300a} \tag{93}$$

Hence it would be possible to determine magnetic field strengths by only measuring particle flux as functions of energy and of the relative displacement of the instrument.

Determining the particle lifetime in a swept environment

The existence of a hole in the radiation belt can be used to determine particle lifetimes in a swept environment. The transient response of an impulsive injection may be observed, as generally described in Section III. Another method simply calculates the lifetime from observed data. Assuming this to be the case, τ_S is solved from any one of the equations already given.

$$\tau_S = \frac{4\pi^2 r_e R_S \Delta}{A_S \beta c} \qquad (d < a < \Delta, \text{ center of band}) \tag{78}$$

$$\tau_S = \frac{4\pi^2 r_e^2}{A_S \beta c} \sqrt{a R_S} \qquad (d < a < \Delta, \text{ edge of band}) \tag{82}$$

$$\tau_S = \frac{4\pi}{45} \left(\frac{Mc^2 \gamma R^2}{c}\right) \left(\frac{r_e}{R}\right)^5 \frac{1}{A_S} \qquad (a > \Delta) \tag{72}$$

Solution of τ_S, however, may not be an end in itself but only a step towards the determination of the injection function q_o.

Determination of the injection function q_o

The particle flux j, has been indicated previously as resulting from a balance between injection and loss.

$$j = nv = (q_o \tau)\ v \tag{94}$$

$$\therefore q_o(E) = j(E)/\beta c\tau \tag{95}$$

In the swept region, $\tau = \tau_S$

$$\therefore q_o(E) = j(E)/\beta(E)\ \ c\,\tau_S(E) \tag{96}$$

Having solved for $\tau_S(E)$, measured j(E) and knowing $\beta(E)$, the injection function can be determined. Such knowledge aids in determining the original source of the radiation belts of the earth and other planets.

Determining the effective atmospheric density

Considerable work has been done on the lifetime of particles in a planetary atmosphere. Since $\frac{dE}{dt} \sim \rho E^{-1/2}$ proton lifetimes are proportional to $E^{1.5}$ and ρ^{-1}, where ρ is the density of effective free electrons. Since

$$j_{1/e} = q_o\, \tau_{1/e}, \tag{97}$$

flux measurements away from the swept region and knowledge of q_o reveal the lifetime ($\tau_{1/e}$) of the particles for a given energy range. Therefore, the atmospheric equivalent electron density can be solved from:

$$\tau_{1/e} = 6.7 \times 10^{10}\ E^{1.5}/\rho \text{ sec.} \tag{98}$$

In this equation E is the particle energy in Mev. A hydrogen ion atmosphere is assumed.

In summary, it can be seen that a vast amount of information about the radiation belt, its source, the average planetary atmosphere, the magnetic field, and the sweeper can be obtained from measurements of only a few parameters. The Martian satellite Phobos presents a very interesting application of these principles. If Mars has a radiation belt, measurements of the flux intensities would be quite revealing. These data would reveal properties of the Martian magnetic field and the diameter of Phobos directly.

C. Fission Electrons from Starfish

An example of artificial injection which can be used to observe radiation lifetimes is the high altitude nuclear explosion "Starfish." This event took place July 9, 1962, 400 km over Johnson Island in the Central Pacific Ocean. The yield was 1.4 MT, resulting in the release of fission fragments which deposited energetic electrons in the upper atmosphere. The resultant distribution has been observed by several satellites and a number of papers treating the interpretation of the data have been written.

Measurements of electron flux by "Injun" showed that the intense part of the artificially created electron belt at several Mev resembled a thin crescent, centered on the magnetic shell L=1.2. The intensity of the belt was only 10% of this value at L=1.8, and 1% at L=2.2 (Hess 1963). A low-altitude polar satellite measured electrons with fission-like spectra above 2 Mev in the region of the South Atlantic magnetic anomaly. Comparisons of data 1 week after the event indicated electron lifetimes in excess of 20 days ($1.16 < L < 1.60$, $0.20 < B < 0.22$). Near L=4.5, B = 0.4 gauss, only natural electrons were observed. The peak flux measured was 1×10^{8} electrons cm^{-2} sec^{-1} at B = 0.20 gauss, and L = 1.20 (Moyer, et al 1963). Data taken by a geiger counter on the TRAAC satellite 1 hour and 9 1/2 hours after the event showed a decay factor on the order of 50 for flux observed at B = 0.230 gauss and L = 1.216 (Pieper, et al 1963). Welch, Kaufman and Hess (1963) show that this

early decay follows the form $\tau/(t + \tau)$ which later becomes an ordinary exponential decay. For L = 1.25, τ varies from 10^4 sec at B = .21, to 10^7 sec at the equator, as a result of atmospheric scattering and energy loss. The exponential decay for L = 1.25 has a mean life of 1.3×10^8 seconds. Figure 20 shows the calculated decay of electrons on the shell L = 1.25 for E = 2.25 Mev (Welch, et al 1963) . The successive curves indicate the natural decay of electrons due to atmospheric losses. It is interesting to note the rapid decay of electrons with small pitch angles which penetrate more deeply into the atmosphere. Electrons which remain near the equator are only slightly reduced in number in the same time period.

If it were assumed that a sweeper satellite of substantial cross section passed through the artificial electron belt, the time variation of the electron flux would be different than that based on atmospheric effects. Assuming the artificial electrons of energy 2.25 Mev, to be centered on the shell L = 1.25, the appropriate lifetime expression in a swept environment is taken from part A of this section:

$$\tau_s = 4\pi^2 R_s r_e \Delta \left[1 - \frac{(R_s^2 + \Delta^2 - r_e^2)^2}{4R_s^2 \Delta^2} \right]^{1/2} / A_S \beta c. \qquad (99)$$

For $R_s = r_e = 1.25R$, $\Delta = 0.063R$ and $\beta = 0.99$

$$\tau = 5.0 \times 10^{16} / A_S \qquad (100)$$

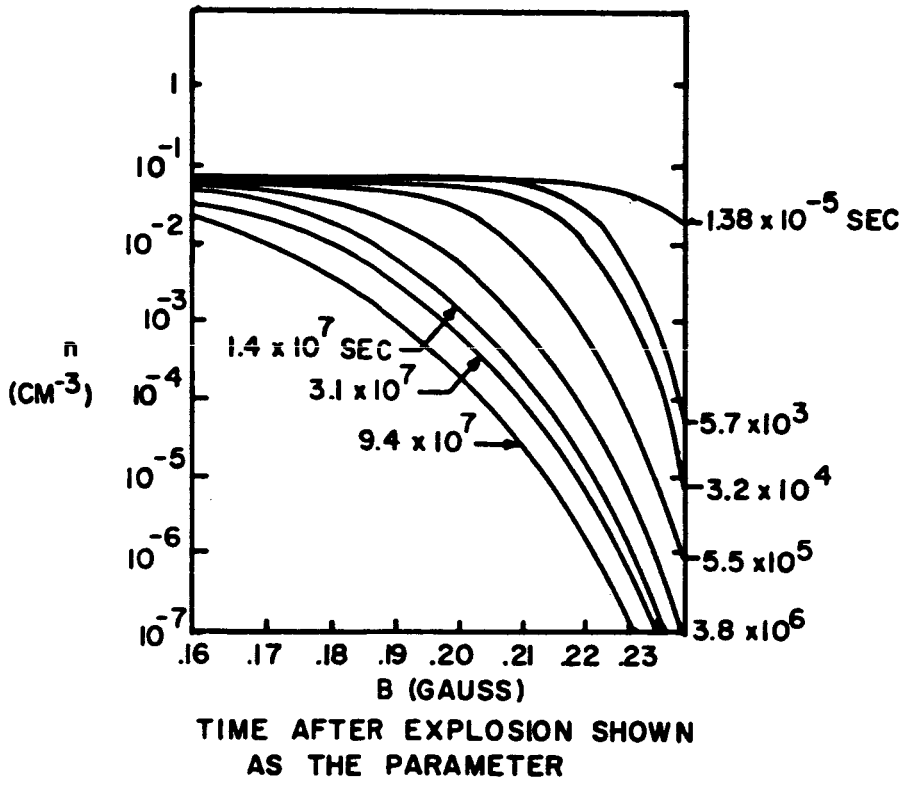

Figure 20. Calculated Decay of Starfish Electrons (L = 1.25, E = 2.25 Mev) (from Welch, et al. (1963))

In order to have a lifetime on the order of 1 year, (less than the average 1.3×10^8 second life of electrons on shell L = 1.25), it is required that $A_S \approx 2 \times 10^9 = 2 \times 10^5 m^2$. While this sweeper area is admittedly rather large from a practical standpoint, the sweeping principle is nevertheless valid. The resultant decay of electrons would be exponential as indicated in Section III. Not only would artificial electrons be swept up by the satellite or satellites, but so would natural electrons and protons as well. This would result in a depression of the radiation flux below the natural level in the vicinity of the sweeper.

The relative decay of the "Starfish" electrons by atmospheric processes is compared to the decay by satellite sweeper action in Figure 21. Electrons which travel down a line of force to large values of field strength are quickly absorbed by the atmosphere resulting in the dip in the concentration as shown in Figure 20. The sweeper action absorbs electrons of a wide range of pitch angles almost uniformly. As a result, the concentration decays uniformly with respect to pitch angle except where atmospheric losses predominate, namely at high values of B as shown in Figure 21. The pitch angle dependence is weak and is not readily observed in the scale of these figures. The tendency is to reduce the concentration near the equator by a factor of less than two. It is predicted that a sweeper with a cross section of 2×10^5 m^2 could reduce the total quantity of injected electrons to about $5 \times 10^{-4} cm^{-3}$ or slightly better than 10^{-3} times the original concentration in 10 years.

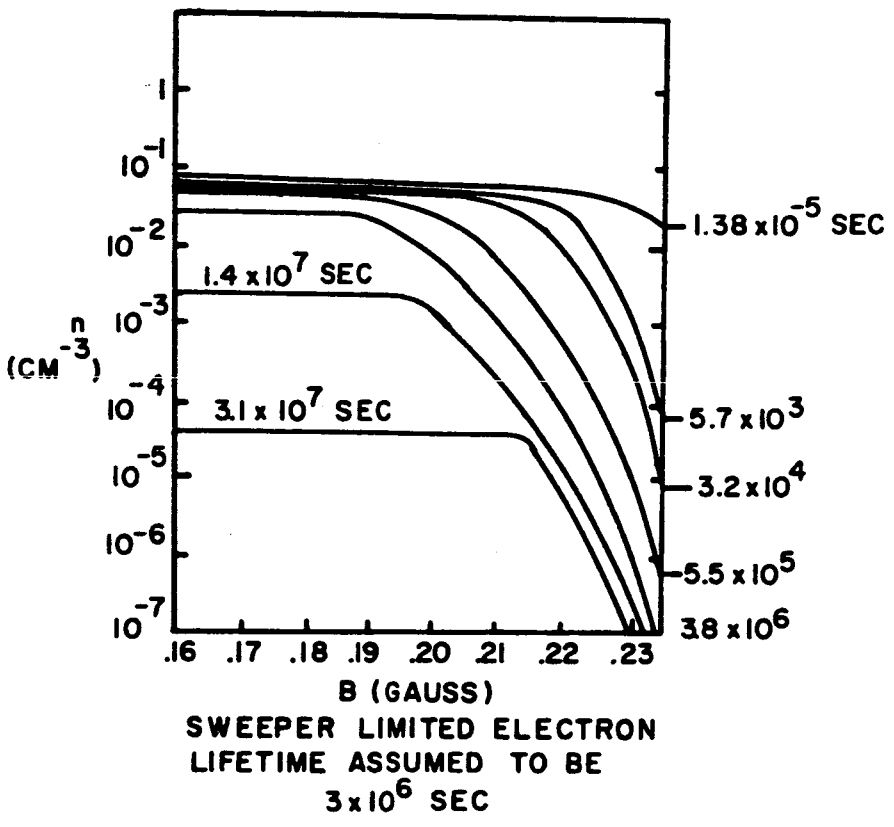

Figure 21. Comparison of Natural Decay and Hypothetical Sweeper Decay of Starfish Electrons

This compares to a reduction by about 5 to 10 times from atmospheric processes.

D. Modulation of the Atmosphere

It has been shown that the radiation lifetime as set by atmospheric losses is inversely proportional to the atmospheric density (Singer and Lenchek 1962). In many problems concerning radiation lifetimes it is suitable to assume an average atmosphere. When radiation flux measurements are used to deduce atmospheric properties, however, the time variations in the atmosphere must be taken into account. As will be shown, the particle lifetime and the time scale of the atmospheric variation will effect observations.

The principal variations of the atmospheric density are the diurnal variation, the 27-day variation, and the 11-year solar cycle. The diurnal density variation, arising from the earth's rotation, has been detected by satellite orbit observations (Jacchia 1960). This variation appears as a bulge in the atmosphere which extends outward, in the general direction of the sun. The 27-day and 11-year variations in the average density of the atmosphere, are caused by the rotation and the activity of the sun.

Since the radiation lifetime has been described in terms of an atmospheric density, the proper density value is the average value experienced by a particle over its lifetime. Because of the variations just described, the proper average density depends on the particle's lifetime,

the time scale of the variation, and the phase of the cycle at the time of observation. The actual behavior of the atmospheric variations can be described by a Fourier series. In some particular cases, a single component adequately describes the variation.

Examining one such case, the instantaneous atmospheric density is assumed to be given by

$$\rho = \rho_o \left[1 + \epsilon \sin(\omega t + \theta)\right] \tag{101}$$

where

ρ_o = average atmospheric density

ϵ = fractional variation

ω = angular frequency of variation

θ = phase of cycle at t = o

Averaged over a time τ, the averaged density is $\bar{\rho}$.

$$\bar{\rho} = \rho_o \left[1 + \frac{\epsilon}{\omega\tau} \left(\cos\theta < [1 - \cos\omega\tau\ ] + \sin\theta \sin\omega\tau \right)\right] \tag{102}$$

For $\omega\tau \ll 1$

$$\bar{\rho} \approx \rho_o \left[1 + \epsilon \left(\sin\theta + \frac{\omega\tau}{2} \cos\theta\right)\right] \tag{103}$$

Therefore, the average density lies between the limits of

$$\rho_o \left[1 + \frac{\omega\tau}{2} \epsilon\right] \leq \bar{\rho} \leq \rho_o \left[1 + \epsilon\right] \tag{104}$$

For $\omega\tau \gg 1$

$$\bar{\rho} \approx \rho_o \tag{105}$$

It should be noted that for $\omega\tau = 2\pi$ or exact multiples thereof, the averaged density is equal to ρ_o. The averaged density ($\bar{\rho}$) is shown as a function of $\omega\tau$ in Figure 22.

In general it is noted that when $\omega\tau << 1$, that is when the lifetime of a certain group of observed particles is much shorter than the time scale associated with the variation in question, the averaged density experienced by these particles is essentially the density existing at the time of the observation. For a different group of particles with a lifetime considerably longer than the period of the variation ($\omega\tau >> 1$), the averaged density ($\bar{\rho}$) is approximately equal to the average density (ρ_o) which the variation occurs.

For particles with lifetimes in between these two cases, the averaged density will reflect the characteristics of the variation. There are two important consequences. The first is that if present or fairly recent atmospheric densities were to be deduced from radiation flux measurements, then a suitably short-lived particle must be selected for observation. This would suggest low energy particles at very high altitudes or higher energy particles at lower altitudes (Singer, 1963). The second is that by taking measurements throughout the energy spectrum, the averaged air density experienced by particles of successively longer lifetimes could be used to reconstruct theoretically the prior history of the atmosphere. It would be possible for instance to deduce atmospheric densities from the present time back some hundreds of years, assuming

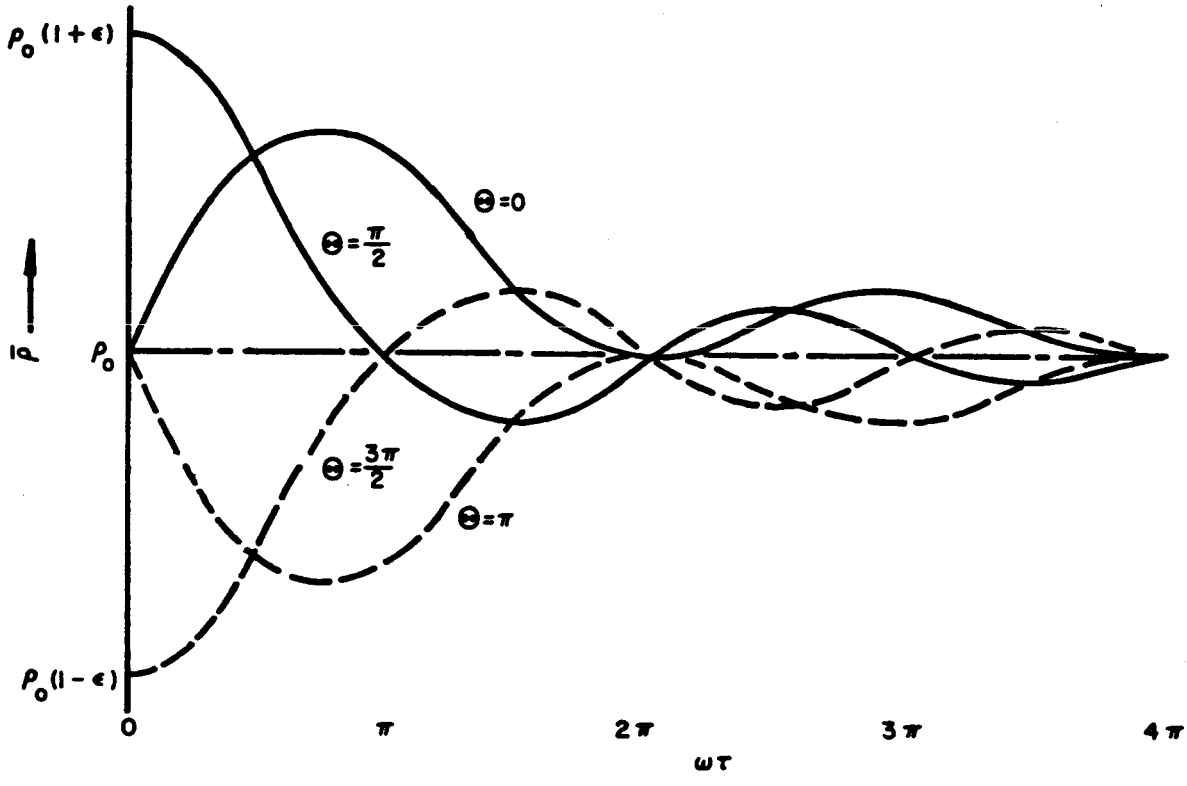

Figure 22. Averaged Atmospheric Density $\overline{\rho}$ vs $\omega\tau$

an injection function could be approximated for a similar time period. It has been determined that the longest life for very energetic protons found in some parts of the atmosphere is about 600 years (Singer (1963)).

It is interesting to note too, that each group of particles having a given lifetime acts as an information filter. Since the actual variation of the atmosphere can be considered to consist of the sum of simple harmonic variations of succeedingly higher frequencies, the effect of the variation of the high frequency components is attenuated by the factor $(\omega\tau)^{-1}$. Therefore, considering particles with a given lifetime, high frequency modulations would be attenuated, so that only the average value ρ_o plus the effect of low frequency modulations would be detected. As an example, particles with lifetimes on the order of 22 years or more could be used to deduce the average density (ρ_o) for the past solar cycle, filtering out the diurnal and the 27-day variations. Using a "1-year" particle would allow the magnitude of the 11-year variation to be deduced without complication from the 27-day variation owing to an adequate frequency separation (12:1). The variation would be determined by correlating one of the first maxima of Figure 22 with $\epsilon\rho_o$ of equation (101). A case in point is a summary of data on time variations of proton fluxes in the inner belt (Freden (1963)). Comparison of proton flux data for the 1959-1960 time period with data for 1962-1963 shows some changes in the proton fluxes on magnetic shells between $L \approx 1.30$ and $L = 1.80$

at relatively low mirror altitudes. Freden reaches the following conclusions:

"(1) At L = 1.4, the shape of the proton spectrum above ≈ 60 Mev has not changed appreciably during the 1959-1963 period. Below ≈ 60 Mev, the results suggest an increase in the flux at ≈ 10 Mev but this conclusion is very uncertain.

"(2) At L = 1.8, solar proton events appear to contribute to the proton flux at ≈ 10 Mev. Other time variations due to the changing atmospheric densities may also manifest themselves to a large degree at these low energies.

"(3) There appears to be an increase in the absolute omnidirectional proton flux above ≈ 30 Mev over the time period 1958-1962 at some B and L values but the magnitude of the increase and its spatial dependence are very much in question. The accompanying table lists a summary of these results:

TABLE V*

OBSERVED PROTON FLUX VARIATIONS WITH TIME

Source	Proton Energy (Mev)	Time Period	B, L	Flux Ratio
Pizzella (Exp. VII)	>30	Oct. '59 - Dec. '60	.22, 1.25-1.6	3
McIlwain (Exp. XV)	>30	Nov. '62 - Jan. '63		1.25
Filz (USAF)	>55	Aug. '61 - June '62	.22, 1.4	1

* Freden (1963)

TABLE V (Continued)

Source	Proton Energy (Mev)	Time Period	B, L	Flux Ratio
McIlwain (Exp. IV)	>30	58/59 - 62/63	.22, 1.4	2
McIlwain (Exp. XV)			.20, 1.4	1
McIlwain (Exp. IV)	>30	58/59 - 62/63	.22, 1.4	2
Freden (USAF)			.20, 1.4	1
McIlwain (Exp. IV)	>30	58/59 - 60	.22, 1.4	2.5
Naugle (Argo D-8)				
Naugle (Argo D-8)	≈10	59/60 - 62/63	.23, 1.8	1/20
Freden (USAF)				

Freden's compilation, given in Table V, indicates changes in proton fluxes above 30 Mev ranging between zero and a factor of three. At the same time the flux decreased at ≈ 10 Mev for L = 1.8. Changes on L = 1.4 would be expected to be affected by atmospheric variations while magnetic distrubances and solar proton events would show a greater effect on shells with L = 1.7 and higher (Singer and Lenchek (1962)). This may account for the great variability of 10 Mev protons at L = 1.8.

Since the elapsed time between initial and later observations is on the order of several years in most of these cases, the significant atmospheric variation is that due to the 11-year solar cycle. Consequently, the data can be interpreted in terms of the atmospheric

densities averaged over appropriate particle lifetimes, terminating at two different phases of the solar cycle.

A summary of the observed data and the results of calculations for these flux variations are shown in Figure 23. These are explained as follows.

The first of Freden's conclusions indicated no change in flux above 60 Mev, and a possible increase at 10 Mev for the 1959-1963 era. Calculating an average air density ($\bar{\rho}$) on the shell L = 1.4, it is found that for E $\approx$ 60 Mev, $\tau \gtrsim 4$ years. The phases of the solar cycle corresponding to 1959 and 1963 are $\pi/2$ and $5\pi/4$ respectively. For $\tau \gtrsim 4$ years, $\omega\tau > 3\pi/4$. Referring to Figure 22, it is noted that $\bar{\rho}$ decreases in this period. Therefore an increase in flux would be expected. For lifetimes in excess of 11 years, theory indicates a smaller decrease in density, allowing a slight increase in proton flux, but this is quite small, especially for E > 117 Mev, corresponding τ = 11 years.

For E $\approx$ 10 Mev, $\tau \approx .3$ years. Referring to Figure 22 it is noted that the averaged density ($\bar{\rho}$) decreases from $\theta_1 = \pi/2$ to $\theta_2 = \frac{5\pi}{4}$. The resultant increase in flux is in agreement with the conclusions of Freden.

The second point made was that atmospheric variations may be felt by low energy protons for B = .23, L = 1.8. Calculating an average density (the method is given in Appendix B) it is found that $\tau \approx .6$ years for E = 10 Mev. Therefore $\omega\tau \ll 1$ and, as may be noted from Figure

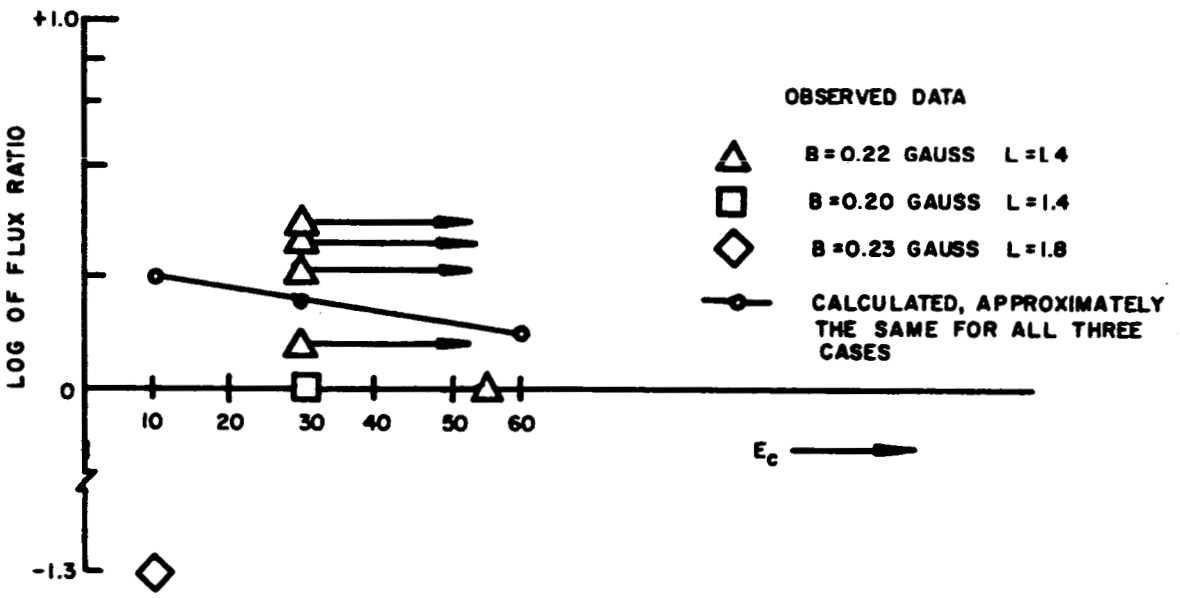

Figure 23. Proton Flux Variations

22, a significant change in averaged density in the time from 1959 to 1963 may be expected. Therefore the flux variation also would be significant and indeed, atmospheric affects might be observed on the shell L = 1.8.

The third statement indicates a wide range of values for the flux change for E > 30 Mev. For B = 0.22 and L = 1.4, the lifetime corresponding to E = 30 Mev is found to be 1.4 years. Therefore $\omega\tau > \frac{\pi}{4}$ and the averaged densities decrease over the time period from $\theta_1 = \frac{\pi}{2}$ to $\theta_2 = \frac{5\pi}{4}$ of the solar cycle. The flux would accordingly increase, in agreement with the data. The magnitude of the change would be about 1.6ϵ, where ϵ is the fractional peak variation in the atmospheric density. For $\epsilon \approx 40\%$, changes in flux on the order of 60% would be expected. The flux ratio then would be 1.6 which compares well with the values zero to 3.0 compiled by Freden.

The low energy component, $E \approx 10$ Mev, has an averaged lifetime of about 0.3 years. For $\omega\tau \approx .06\ \pi$, it would be expected that the density would show a decrease, allowing the flux to increase. The data shows a decrease in flux however. This might be explained by hydromagnetic disturbances since the shell in question, L = 1.8, reaches regions of the magnetosphere where magnetic field distrubances become significant. Solar proton events, as suggested by Freden, might also contribute to this.

E. Conclusions

The lifetimes of the trapped particles in the radiation belts are known to be time dependent. One of the principal sources of this variation is the modulation of the atmosphere. The time scales of these variations range from one day to about eleven years. As a result, the averaged atmospheric density experienced by any given particle over its lifetime is a function of its location in the geomagnetic coordinates, its lifetime, and the time scales of the modulations. Consequently, in the process of deducing atmospheric properties from radiation flux measurements, appropriate energy levels must be chosen in order to obtain the averaged density for a desired era. Low energy particles would yield data on recent atmospheric densities while higher energy particles would be associated with the averaged density over a longer, and therefore earlier period.

The factors contributing to the natural lifetimes and to their variations can be studied by observing the decay of artificially injected particles, such as those from "Starfish." In addition, the sweeping effects of artificial or natural satellites can be utilized to derive more information about the radiation belt, e.g., properties of the radiation belt particles, including the injection function; about the planetary magnetic field, and about atmospheric densities, as this paper has shown.

APPENDIX A

B-L COORDINATES

A feature of the earth's magnetic field that allowed much of the original analysis of the motion of charged particles to be developed is its close resemblance to a dipole. As instrumented satellites gathered data on the radiation fluxes it became apparent that the resemblance was not close enough. Because of large flux gradients, even small irregularities in the magnetic field made flux contours in a dipole coordinate system appear disordered.

McIlwain (1961) developed a coordinate system which removes this difficulty. Basically, every point in space lies on a particular magnetic shell. Each shell is identified by its "L" value. (In a pure dipole field the L value for any given shell is simply its equatorial distance in terms of earth radii.) Each shell consists of a line of force rotated about the magnetic axis as shown in Figure 24. In the real field, McIlwain identifies the shells as follows. The reduced longitudinal (second) invariant ($I' = I/mv = \oint\sqrt{1 - B(Z)/Bm}\, dz$) in a dipole field at magnetic latitude λ on a line of force having an equatorial radius r_e is given by

$$I' = r_e f_1(\lambda) \qquad (106)$$

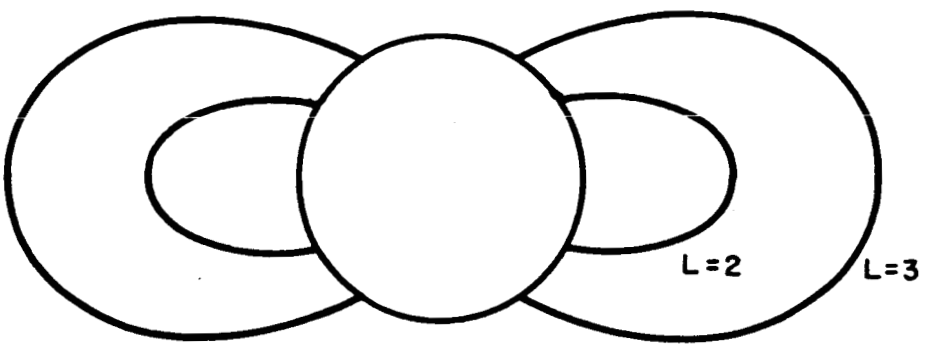

Figure 24. Magnetic Shells in a Dipole Field

In a dipole field, the field strength is a function of the equatorial distance to the line of force, the latitude of the point on the line and the magnetization of the earth. Therefore rearranging the equation for the dipole field, the latitude terms can be separated:

$$B = B\,(r_e,\ M_e,\ \lambda) \tag{107}$$

$$\frac{r_e^{\,3} B}{M_e} = f_2(\lambda) = \frac{(4 - 3\cos^2\lambda)^{1/2}}{\cos^6\lambda} \tag{108}$$

Combining equations (106) and (108)

$$\frac{I'^3 B}{M_e} = \frac{r_e^{\,3} B}{M_e}\ f_1^{\,3}(\lambda)$$

But latitude λ is related to the field strength, magnetization, and equatorial radius by the dipole equation. Therefore $f_1(\lambda)$ can be replaced by an equivalent function.

$$\frac{I'^3 B}{M_e} = \frac{r_e^{\,3} B}{M_e}\ f_3^{\,3}\left(\frac{r_e^{\,3} B}{M_e}\right) \tag{109}$$

The two groups of terms on the right-hand of this equation can be reduced to yet another function.

$$\frac{I'^3 B}{M_e} = f_4\left(\frac{r_e^{\,3} B}{M_e}\right) \tag{110}$$

Conversely,

$$\frac{r_e^{\,3} B}{M_e} = F\left(\frac{I'^3 B}{M_e}\right) \tag{111}$$

The real magnetic shell containing the point where the field is B on the line of force for which I' was evaluated is identified by L, where L replaces r_e in the above expression. Therefore

$$\frac{L^3 B}{M_e} = F\left(\frac{I'^3 B}{M_e}\right) \tag{112}$$

The function F into which the real field values of I' and B are inserted is the function derived from a dipole field. Values of F have been tabulated by McIlwain over a wide range. These are shown in Table VI. For any given value of B and L in the real field, its corresponding point in a dipole field can be found from the dipole equations

$$B = \frac{M_e}{r^3}\left(4 - \frac{3r}{L}\right)^{1/2} \tag{113}$$

$$r = L\cos^2\lambda \tag{114}$$

These equations are plotted in Figure 25.

TABLE VI

MCILWAIN'S COORDINATE TRANSFORMATION

$I^3 B/M$	$L^3 B/M$	$I^3 B/M$	$L^3 B/M$
2.37529×10^{-15}	1.00002	1.74352×10^{-6}	1.01632
1.72697×10^{-12}	1.00016	4.41257×10^{-6}	1.02228
3.70298×10^{-11}	1.00045	9.87364×10^{-6}	1.02919
2.37086×10^{-9}	1.00180	2.01130×10^{-5}	1.03707
2.70390×10^{-8}	1.00406	3.80506×10^{-5}	1.04596
1.52215×10^{-7}	1.00722	6.78113×10^{-5}	1.05585
5.82114×10^{-7}	1.01131	1.15409×10^{-4}	1.06680

TABLE VI (Continued)

I^3 B/M	L^3 B/M	I^3 B/M	L^3 B/M
1.87314×10^{-4}	1.07881	3.01912×10^{-1}	2.13036
2.94482×10^{-4}	1.09194	3.59672×10^{-1}	2.21352
4.49250×10^{-4}	1.10620	4.27504×10^{-1}	2.30245
6.67702×10^{-4}	1.12165	5.07058×10^{-1}	2.39766
9.69961×10^{-4}	1.13832	6.00263×10^{-1}	2.49967
1.38095×10^{-3}	1.15626	7.09352×10^{-1}	2.60911
1.93121×10^{-3}	1.17553	8.36934×10^{-1}	2.72664
2.65795×10^{-3}	1.19618	9.86054×10^{-1}	2.85300
3.60595×10^{-3}	1.21827	1.16025	2.98905
4.82943×10^{-3}	1.24187	1.36367	3.13571
6.39281×10^{-3}	1.26706	1.60116	3.29403
8.37277×10^{-3}	1.29392	1.87843	3.46520
1.08602×10^{-2}	1.32252	2.20216	3.65056
1.39624×10^{-2}	1.35298	2.58020	3.85161
1.78056×10^{-2}	1.38538	3.02183	4.07005
2.25380×10^{-2}	1.41985	3.53799	4.30783
2.8332×10^{-2}	1.45650	4.14164	4.56716
3.53938×10^{-2}	1.49547	4.84816	4.85057
4.39567×10^{-2}	1.53691	5.67587	5.16095
5.42973×10^{-2}	1.58097	6.64657	5.50164
6.67358×10^{-2}	1.62782	7.78642	5.87648
8.16455×10^{-2}	1.67767	9.12860	6.28994
9.94598×10^{-2}	1.73070	1.07055×10	6.74720
1.20681×10^{-1}	1.78716	1.25680×10	7.25432
1.45983×10^{-1}	1.84729	1.47699×10	7.81840
1.75772×10^{-1}	1.91135	1.73787×10	8.44781
2.11103×10^{-1}	1.97966	2.04766×10	9.15245
2.52798×10^{-1}	2.05255	2.41655×10	9.94413

TABLE VI (Continued)

I^3 B/M	L^3 B/M	I^3 B/M	L^3 B/M
2.85705×10	1.08369×10	1.90201×10^3	1.79669×10^2
3.38471×10	1.18478×10	2.23574×10^3	2.04483×10^2
4.01899×10	1.29973×10	2.64005×10^3	2.34175×10^2
4.78427×10	1.43104×10	3.14300×10^3	2.70014×10^2
5.71146×10	1.58179×10	3.76361×10^3	3.13689×10^2
6.83985×10	1.75576×10	4.55081×10^3	3.67477×10^2
8.21991×10	1.95767×10	5.54426×10^3	4.34504×10^2
9.91695×10	2.19347×10	6.83524×10^3	5.19133×10^2
1.20162×10^2	2.47069×10	8.51087×10^3	6.27578×10^2
1.46301×10^2	2.79896×10	1.07567×10^4	7.68892×10^2
1.79085×10^2	3.19079×10	1.37789×10^4	9.56603×10^2
2.20532×10^2	3.66255×10	1.79974×10^4	1.21153×10^3
2.45179×10^2	3.93495×10	2.39555×10^4	1.56683×10^3
2.73402×10^2	4.23601×10	3.27489×10^4	2.07743×10^3
3.05069×10^2	4.56967×10	4.60402×10^4	2.83877×10^3
3.41513×10^2	4.94049×10	6.73169×10^4	4.02645×10^3
3.82642×10^2	5.35387×10	1.02942×10^5	5.98740×10^3
4.30241×10^2	5.81615×10	1.67841×10^5	9.47159×10^3
4.84311×10^2	6.33486×10	2.96984×10^5	1.63048×10^4
5.47285×10^2	6.91896×10	5.95512×10^5	3.17247×10^4
6.19343×10^2	7.57921×10	1.44453×10^6	7.49153×10^4
7.03884×10^2	8.32855×10	5.00559×10^6	2.51887×10^5
8.01427×10^2	9.18267×10	1.47748×10^7	7.32706×10^5
9.16824×10^2	1.01607×10^2	4.09266×10^7	2.00752×10^6
1.05125×10^3	1.12862×10^2	1.91226×10^8	9.28013×10^6
1.21182×10^3	1.25883×10^2	6.50554×10^8	3.12969×10^7
1.40095×10^3	1.41032×10^2	5.20779×10^9	2.50188×10^8
1.62942×10^3	1.58767×10^2		

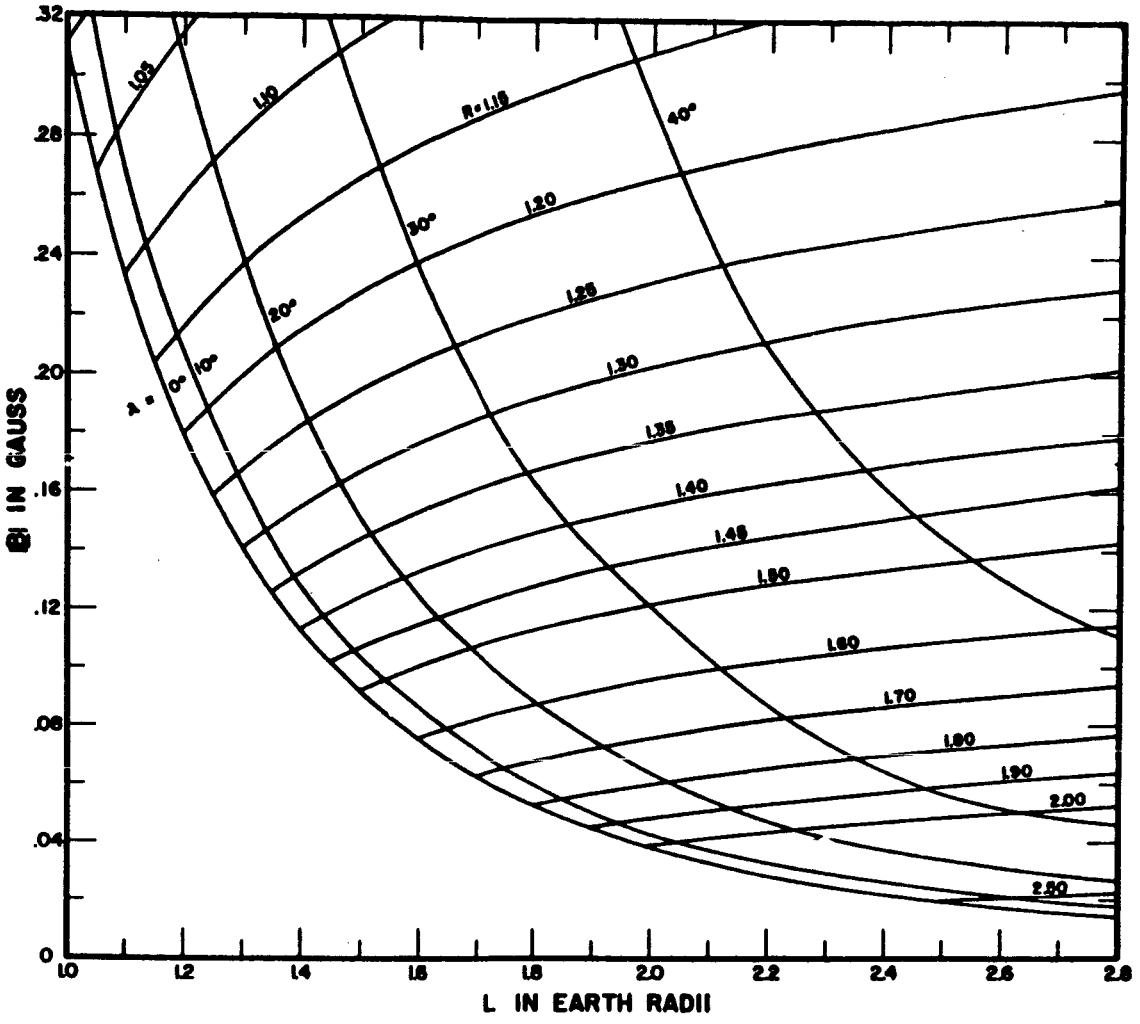

Figure 25. Magnetic Coordinates for a Dipole Field

When McIlwain's coordinate transformation is used in conjunction with integral invariant values for different lines of force and magnetic latitudes, the motion of trapped particles can be followed in geographic coordinates. This is especially useful, for instance, in determining the actual atmospheric density to which a given trapped particle may be exposed.

APPENDIX B

AVERAGE DENSITY

Because of distortions in the earth's magnetic field, the average atmoshperic density along the trajectory of a trapped particle is not easily obtained. It can be calculated, however, by averaging over each of a number of lines of force on a given shell, between appropriate mirror points, and then averaging that result over the azimuthal drift. As the following will show, the actual average density is a factor or so different from that which a pure dipole model would yield.

For a dipole field, Ray (1960) has shown that the average atmospheric density on a line of force, and therefore for the entire shell, is given by:

$$\bar{\rho} = \rho_m \frac{1}{S(\mu)} \left[\frac{\pi}{6} \frac{H}{r_e} \frac{X_m (4 - 3X_m)^2}{(8 - 5X_m)(1 - X_m)} \right]^{1/2} \tag{115}$$

where

ρ_m = mirror point density

$X_m = r_m / r_e$

r_m = geocentric radius of mirror point

$S(\mu)$ = dimensionless spiral path length

H = atmoshperic scale height

This holds for mirror points below the transition altitude in the exosphere (1000-1200 km), where oxygen is predominant.

The following density calculation is for the shell L = 1.297 with mirror point at B = .186 gauss, which has a minimum altitude of about 700 km located at latitude 27°S and longitude 40°W. It is assumed that the field distortion causes the density to vary from that of a dipole model primarily in the azimuth coordinate and that the variation from a dipole model over a line of force is a smaller effect. Consequently, for each mirror point, an average density can be computed from the actual mirror point density, the actual scale height, and geometrical factors ($S(\mu)$, X_m) based on a dipole model. These are shown in Table VII.

The altitude variations of the mirror point as longitude varies was obtained from graphical charts of Dudziak et al (1963). A typical trace is shown in Figure 26. The average atmosphere, from Singer and Lenchek (1962), is shown in Figure 27. The atmoshperic scale height was averaged over the diurnal period and the solar cycle from data of Harris and Priester (1962). Ray's formula was modified by substituting r_m/X_m for r_e in order to keep parameters in terms of actual altitude as much as possible. The final results are summarized in Table VIII.

The density at the mirror points in the real field varies from 0.20×10^5 to 22.0×10^5 cm^{-3} whereas the dipole model mirror point density is always 1.15×10^5 cm^{-3}. The average mirror point density in the real field is twice that of the dipole field, because of the dip to

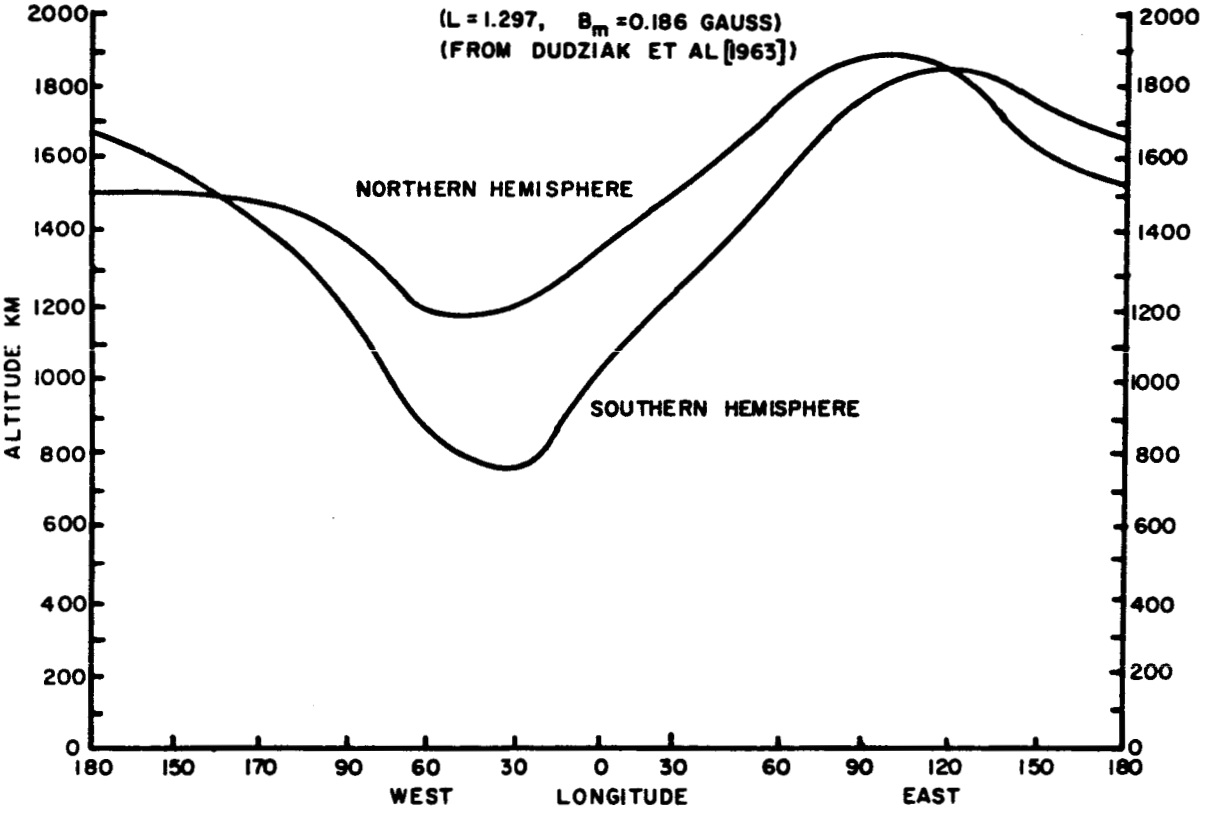

Figure 26. Mirror Point Trace in Real Field

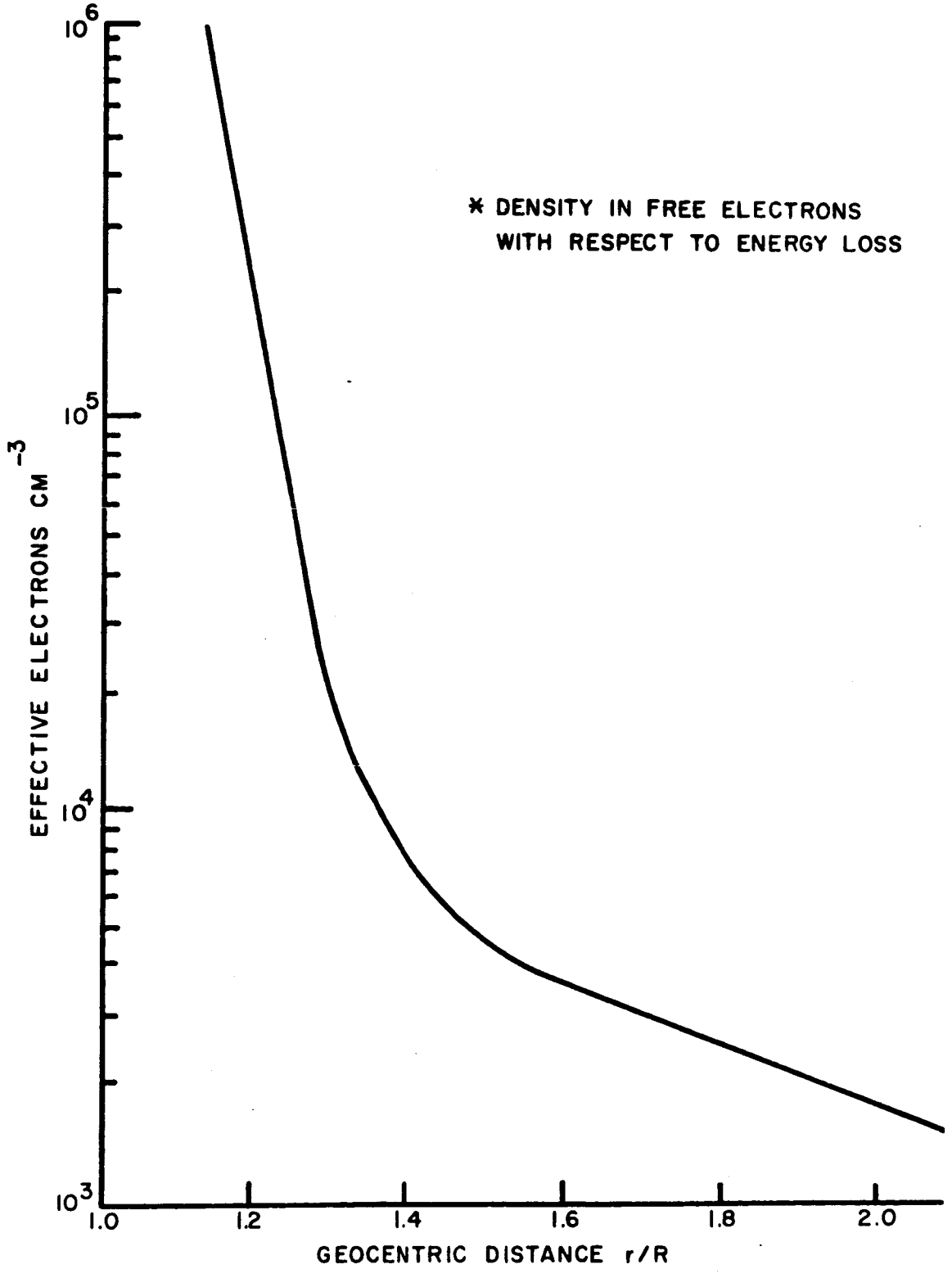

Figure 27. Average Atmospheric Density* vs Geocentric Distance

TABLE VII

AVERAGE ATMOSHPERIC DENSITY (EFFECTIVE ELECTRONS PER cm^3)
ON LINES OF FORCE (L = 1.297, B_m = .186 gauss)

Longitude East	Southern Hemisphere h_m Km	ρ_m cm^{-3}	H_m km	$\bar{\rho}_S$* cm^{-3}	Northern Hemisphere h_m Km	ρ_m cm^{-3}	H_m km	$\bar{\rho}_N$* cm^{-3}	$\bar{\rho}_{NS}$ cm^{-3}
0	1050	5.2×10^5	200	2.65×10^5	1390	1.2×10^5	345	$.74 \times 10^5$	1.70×10^5
15	1190	2.6	280	1.45	1470	.90	350	.57	1.01
30	1300	1.7	280	1.01	1550	.62	390	.44	0.72
45	1390	1.2	350	.74	1640	.46	410	.32	0.53
60	1540	.62	380	.42	1730	.30	425	.24	0.33
75	1700	.36	425	.26	1830	.25	455	.18	0.22
90	1810	.25	460	.19	1900	.20	500	.14	0.16
105	1880	.20	490	.15	1910	.20	510	.14	0.15
120	1875	.20	490	.15	1860	.22	485	.16	0.16
135	1835	.25	470	.17	1775	.30	450	.21	0.19
150	1760	.30	440	.22	1675	.43	425	.29	0.26
165	1710	.37	430	.25	1580	.58	400	.39	0.32
180	1650	.44	400	.31	1510	.76	375	.50	0.41

*Assumes same density at both mirror points, actual $\bar{\rho}_{NS} = \frac{1}{2}(\bar{\rho}_S + \bar{\rho}_N)$

TABLE VII (Continued)

Longitude East	Southern Hemisphere h_m Km	ρ_m cm^{-3}	H_m km	$\bar{\rho}_S$* cm^{-3}	Northern Hemisphere h_m Km	ρ_m cm^{-3}	H_m km	$\bar{\rho}_N$* cm^{-3}	$\bar{\rho}_{NS}$ cm^{-3}
195	1625	.45	410	.34	1500	.76	370	.52	0.43
210	1575	.58	400	.40	1495	.77	365	.53	0.47
225	1525	.75	375	.48	1490	.77	365	.53	0.51
240	1440	.90	350	.63	1485	.77	360	.54	0.59
255	1350	1.3	315	.85	1460	.90	350	.58	0.72
270	1210	2.5	275	1.40	1400	1.20	330	.72	1.06
285	1050	5.2	200	2.65	1290	2.0	300	1.05	1.85
300	850	12.0	150	5.5	1175	3.2	270	1.55	3.55
315	725	22.0	125	9.5	1150	3.3	260	1.70	5.60
330	760	17.0	140	7.5	1210	2.5	275	1.40	4.45
345	900	10.0	175	4.8	1300	1.7	300	1.00	2.90

*Assumes same density at both mirror points, $\therefore$ actual $\bar{\rho}_{NS} = \frac{1}{2}(\bar{\rho} + \bar{\rho}_N)$

TABLE VIII

REAL FIELD AVERAGE DENSITY VS. DIPOLE MODEL DENSITY
($L = 1.297$, $B_m = .186$ gauss)

	Dipole Field	Real Field
Mirror Point Density (cm^{-3})	1.15×10^5	2.2×10^5*
Average Density (cm^{-3})	0.55×10^5	1.18×10^5

*Actual density at mirror points averaged in azimuth

lower altitudes, particularly at the South Atlantic anomaly. The effect of averaging over a line of force, however, reduces the density by a factor of two. Therefore, the average atmoshperic density experienced by particles which mirror at B = .186 on shell L = 1.297 is almost identical to that of the mirror point in a dipole field. While this result cannot be generalized to include all shells, it is assumed to hold for shells with values of $L \approx 1.3$ for which mirror points are near B = .186 gauss.

REFERENCES

Alfvén, H.: Cosmical Electrodynamics, Clarendon Press, Oxford, 1950.

Dudziak, W.F., D.D. Kleineke and T.J. Kostigen: Graphic Displays of Geomagnetic Geometry, (DASA 1372), 1963.

Fan, C.Y., P. Meyer and J.A. Simpson: Trapped and Cosmic Radiation Measurements from Explorer VI, in Space Research (Ed H. Kollman Bijl) (North-Holland Publ.), 1960.

Fermi, E.: Nuclear Physics (notes compiled by J. Orear, A.H. Rosenfeld, and R.A. Schulter) Univ. of Chicago Press, 1960.

Freden, S.C., and R.S. White: Protons in the Earth's Magnetic Field, Phys. Rev. Letters 3, 9, 1959.

Freden, S.C.: Private Communication to S.F. Singer, 1963.

Hamlin, D.A., R. Karplus, R.C. Vile and K.M. Watson: Mirror Frequencies for Geomagnetically Trapped Particles, J. Geophys. Res. 66, 1, 1961.

Harris, I. and W. Priester: Theoretical Models for the Solar-Cycle Variation of the Upper Atmosphere, J. Geophys. Res. 67, 4585, 1962.

Herring, J. and L. Kyle: Density in a Planetary Exosphere, J. Geophys. Res. 66, 1980, 1961.

Hess, W.N.: The Artificial Radiation Belt Made on July 9, 1962, J. Geophys. Res. 68, 667 n, 1963.

Jacchia, L. G.: A Variable Atmospheric Density Model From Satellite Observations, J. Geophys. Res. 65, 9, 1960.

Jensen, D. C., R. W. Murray and J. A. Welch, Jr.: Tables of Adiabatic Invariants for the Geomagnetic Field 1955.0, AFSWC-TN-60-8, 1960.

Jensen, D. C. and W. A. Whitaker: Spherical Harmonic Analysis of the Geomagnetic Field, J. Geophys. Res. 65, 2500, 1960.

Jensen, J., G. Townsend, J. Kork and D. Kraft: Design Guide to Orbital Flight, McGraw-Hill, New York, 1962.

Kellogg, P. J.: Possible Explaination of the Radiation Observed by Van Allen at High Altitudes in Satellites, Nuovo Cim. Suppl. (Ser. 10), 11, 48, 1959.

King-Hele, D. G.: Properties of the Atmosphere Revealed by Satellite Orbits, in Progress in the Astronautical Sciences (Ed S. F. Singer) North-Holland Pub, Amsterdam, 1962.

Lenchek, A. M.: Geomagnetically Trapped Radiation From Fast Cosmic-Ray Albedo Neutrons, Thesis, Univ. of Maryland, 1962.

Massey, H. S. W. and R. L. F. Boyd: The Upper Atmosphere, Philosophical Library, 1959.

McIlwain, C. E.: Coordinates for Mapping the Distribution of Magnetically Trapped Particles, J. Geophys. Res. 66, 3681, 1961.

McIlwain, C. E.: The Radiation Belts, Natural and Artifical, Science 142, 355, 1963.

Mitra, S.K.: The Upper Atmosphere (The Asiatic Society), 1947.

Moyer, F.S., D.D. Elliot, J.D. Mihalov, G.A. Paulikas, A.L. Vanipola and S.C. Freden: Preliminary Analysis of the Fluxes and Spectrums of Trapped Particles After the Nuclear Test of July 9, 1962, J. Geophys. Res. 68, 641, 1963.

Nicolet, M.: The Constitution and Composition of the Upper Atmosphere, IRE Proceedings, 47, 2, 1959.

Northrop, T.G. and E. Teller: Stability of the Adiabatic Motion of Charged Particles in the Earth's Magnetic Field, Phys. Rev. 117, 215-225, 1960.

O'Brien, B.J., J.A. Van Allen, C.D. Laughlin and L.A. Frank: Absolute Electron Intensities in the Heart of the Earth's Outer Radiation Zone, J. Geophys. Res. 67, 397, 1962.

Opik, E.J. and S.F. Singer, Distribution of Density in a Planetary Exosphere, Phys. of Fluids 2, 653, 1959; 3, 486, 1960; 4, 221, 1961.

Pieper, G.F., D.J. Williams and L.A. Frank: Traac Observations of the Artificial Radiation Belt From the July 9, 1962, Nuclear Detonation, J. Geopnys. Res. 68, 635, 1963.

Ratcliffe, J.A.: Physics of the Upper Atmosphere (Academic Press), 1960.

Singer, S.F.: Trapped Orbits in the Earth's Dipole Field, Bull Am. Phys. Soc., Series II, 1, 229(a), 1956.

Singer, S.F.: Trans. Am. Geophys. Union, 38, 175, 1957.

Singer, S.F.: Radiation Belt and Trapped Cosmic Ray Albedo, Phys. Rev. Letters, 1, 171, 1958a.

Singer, S.F.: Trapped Albedo Theory of the Radiation Belt, Phys. Rev. Letters, 1, 181, 1958b.

Singer, S.F.: Some Consequences of a Theory of the Radiation Belt, J. Brit. Interplan. Soc., 16 (10), 558-564, 1958c.

Singer, S.F.: Nuclear Explosions in Space, Nature 196, 307, 1962.

Singer, S.F.: Radiation Belts of Venus and Mars (with consideration of sweeping effect of Phobos), in Space Age Astronomy(Ed. A. Deutsch and W. Klemperer), Academic Press, New York, 1962b.

Singer, S.F.: What Determines the Lifetimes of Protons?, Cospar, Warsaw, 1963.

Singer, S.F. and A.M. Lenchek: Geomagnetically Trapped Radiation, in Progress in Elementary Particle and Cosmic Ray Physics (ed J.G. Wilson and S.A. Wouthuysen), North-Holland Publ. Co., Amsterdam, 1962.

Spitzer, L.: Physics of Fully Ionized Gases, Intersciences Publ., New York, 1962.

Van Allen, J.A., and L.A. Frank: Radiation Around the Earth to a Radial Distance of 107,400 Kilometers, Nature 183, 430, 1959a.

Vernov, S.N., N.L. Grigorov, I.P. Ivanenko, A.I. Lebedenskii, V.S. Murzier and A.E. Chudaliov: Possible Mechanism of Production of Terrestrial Corpuscular Radiation Under the Action of Cosmic Rays,

Sov. Phys. Dokl. 4, 154, 1959; (T) Russian orig; Dokl. Akad Nank. SSSR 124, 1002, 1959.

Welch, J.. A., Jr., R. L. Kaufmann and W. N. Hess: Trapped Electron Time Histories for L = 1. 18 to L = 1. 30, J. Geophys. Res. 68, 685, 1963.

Wentworth, R. C.: Lifetimes of Geomagnetically Trapped Particles Determined by Coulomb Scattering, Thesis, Univ. of Maryland, 1960.